

Electronic Thesis and Dissertation Repository

2-4-2022 2:15 PM

Effective wind area for the design of roof sheathing under wind loading

Nicole E. M. Szilagyi, *The University of Western Ontario*

Supervisor: Kopp, Gregory A., *The University of Western Ontario*

Co-Supervisor: El Ansary, Ayman, *The University of Western Ontario*

A thesis submitted in partial fulfillment of the requirements for the Master of Engineering Science degree in Civil and Environmental Engineering

© Nicole E. M. Szilagyi 2022

Follow this and additional works at: <https://ir.lib.uwo.ca/etd>

Recommended Citation

Szilagyi, Nicole E. M., "Effective wind area for the design of roof sheathing under wind loading" (2022). *Electronic Thesis and Dissertation Repository*. 8390.
<https://ir.lib.uwo.ca/etd/8390>

This Dissertation/Thesis is brought to you for free and open access by Scholarship@Western. It has been accepted for inclusion in Electronic Thesis and Dissertation Repository by an authorized administrator of Scholarship@Western. For more information, please contact wlsadmin@uwo.ca.

Abstract

Wood-frame structures are a popular choice for construction in North America. Due to their sensitivity to severe wind events, the design of these structures under wind loading is of particular importance. One of the issues with wind loading on cladding elements like roof sheathing is the determination of the “effective wind area” to use in design since the design pressure coefficients decrease logarithmically with area. The current design approach for cladding uses a geometric tributary area approach to calculate the wind loads and determine adequate fastening schedules. This fails to include load sharing and design pressure coefficients may be excessively cautious. The objective of the current work is to determine the effective wind area of a roof sheathing panel under three fastening schedules: 6 in by 12 in, 6 in by 6 in, and 3 in by 3 in. It was found that the effective wind area of a $\frac{7}{16}$ in oriented strand board sheathing panel was about 24 sq ft regardless of fastening schedule. This value contrasts with the tributary areas of 2 sq ft, 1 sq ft, and 0.5 sq ft, respectively for the three schedules. However, using the full sheathing panel area of 32 sq ft would be slightly unconservative.

Keywords:

Roof sheathing, wind loading, effective wind area, OSB sheathing, geometric tributary area, finite element modelling, roofs, failure loads

Summary for Lay Audience

In North America wood-frame construction is a popular choice for homes. These structures are vulnerable to extreme windstorms such as hurricanes and tornadoes due to their light weight. Roofs of these structures are particularly high risk due to the large suction loads from these storms. Losing roof sheathing can cause severe water damage and cause further structural failure. To ensure roof sheathing remains attached during these storms it is important for design to be accurate. Current design practices use geometry and capacity of individual fasteners (nails) to determine overall sheathing panel capacity. This practice does not consider any load being shared between fasteners despite the proximity of these connections through the sheathing panel. This thesis looks to quantify the load sharing by determining an effective wind area, the area associated with the failure of the panel. Using finite element modelling software, a model of a single sheathing panel system was constructed. The system included 2 x 4 trusses, fasteners, and a $\frac{7}{16}$ in oriented strand board (OSB) sheathing panel. The model had 3 different fastener orientations a 6 in by 12 in, 6 in by 6 in, and 3 in by 3 in spacing for exterior trusses and interior trusses, respectively. It was tested under 3 load cases including a uniform ramp load, a point ramp load, and a spatially-varying ramp load. Of the 3 tests it was hypothesized that the spatially-varying ramp load would produce the most accurate results for the effective wind area. The effective wind area was calculated based on the total force acting on the panel at initial failure and how many fasteners were engaged at this time for all load cases and fastener orientations. Effective wind area of a sheathing panel was found to be about 24 sq ft.

Acknowledgements

Firstly, I would like to thank my supervisors Dr. Greg Kopp and Dr. Ayman El Ansary for their ongoing support and mentorship. Throughout my degree both have provided a safe and open work environment that allowed me to be successful and grow as a person and a researcher. Their support during the trying times of work from home was unparalleled, especially when I struggled with my mental health. I will forever be grateful for the opportunity to work with both of them.

I would also like to thank the friends I shared an office with including Angela, Caspar, Chris, Connell, Emilio, Sarah, Sam, Matt, and Tsigereda. The office was such a warm and inviting space where we have countless memories and laughs with many of premeeting pep talks and post meeting celebratory drinks, when anxieties ran high. They were able to help me find the words when I could not and fix the errors I couldn't see in my own work. They are supportive in all my endeavors and furthering experiences for everyone no matter where they came from. It has been a pleasure being surrounded by and working with these people.

Lastly, I would like to thank my family and friends. The continued support and show of pride from all of them helped so much when believing in myself was hard. Having my family always remind me my mother would be proud of me and helping me through the degree I told her I would get before she passed. Thank you to my friends for letting me vent when stress was high and helping pick me up when I was down on myself. A special thank you to my Dungeons and Dragons friends that let me escape into a fantasy world and forget about my work for a few hours every week. Finally, a massive thank you to coffee, for helping me in the late nights at the office.

Table of Contents

Abstract.....	ii
Summary for Lay Audience.....	iii
Acknowledgements.....	iv
Table of Contents.....	v
List of Tables.....	vii
List of Figures.....	viii
Nomenclature.....	xi
Chapter 1 Introduction and Background.....	1
1.1 Preface.....	1
1.2 Wind in the Atmospheric Boundary Layer.....	1
1.2.1 Wind Loading on Wood-Frame Homes.....	3
1.2.2 Wind Loading on Sheathing.....	7
1.3 Sheathing Fasteners.....	8
1.3.1 Design Specifications for Sheathing Fasteners.....	8
1.3.2 Capacity of Sheathing Fastener Connections.....	10
1.3.3 Behaviour of Sheathing Fasteners under Wind Loading.....	12
1.3.4 Rate of Loading Impacts on Sheathing Fasteners.....	14
1.4 Roof Sheathing.....	14
1.4.1 Design Specifications for Roof Sheathing Panels.....	14
1.4.2 Capacities of Roof Sheathing Panels.....	15
1.4.3 Failure of Roof Sheathing Panel Systems.....	16
1.5 Objectives.....	19
Chapter 2 Methodology.....	20
2.1 Finite Element Model.....	20

2.1.1	SPF Trusses Using Orthotropic Frame Elements	21
2.1.2	OSB Sheathing Using Orthotropic, Thin Shell Elements	24
2.1.3	Fasteners Using Two Node, Multi-Linear Plastic Links	28
2.1.4	Time History Loading.....	32
2.1.5	Finite Element Model Validation.....	36
2.1.6	Test Matrix and Monte Carlo Simulation	38
Chapter 3 Results and Analysis		41
3.1	Initial Failure Force Results.....	41
3.2	Effective Wind Area	45
3.3	Design Procedure	54
Chapter 4 Conclusions and Recommendations.....		56
References		59
Curriculum Vitae		63

List of Tables

Table 1: SPF Truss Orthotropic Frame Element Material Property Data.....	23
Table 2: OSB Sheathing Shell Element Orthotropic Property Data.....	27
Table 3: Extrapolated ASCE 7-16 GCP values for zone 3 of hip roofs of pitch 27° to 45° with height less than 60 ft (18.3 m)	36
Table 4: Experiment Test Matrix.....	40
Table 5: Failure force results for 6 in by 12 in fastener spacing.....	43
Table 6: Failure force results for a 6 in by 6 in fastener spacing.....	44
Table 7: Failure force results for a 3 in by 3 in fastener spacing.....	45
Table 8: Number of Links and Geometric Tributary Area Based on Location	48
Table 9: 6 in by 12 in Link Spacing Effective Wind Area Calculation Summary using Mean Values	50
Table 10: 6 in by 6 in Link Spacing Effective Wind Area Calculation Summary using Mean Values	51
Table 11: 3 in by 3 in Link Spacing Effective Wind Area Calculation Summary using Mean Values	52
Table 12: Comparison of Current Code Practice and Proposed Effective Wind Area Method for a 6 in by 12 in Fastening Schedule.....	53

List of Figures

Figure 1: Mean wind velocity profile for various surface friction and terrain (Davenport, 1964) 2

Figure 2: Spatial gradient contours for external wind pressures on the roof of the test house. A: External pressure coefficients from wind tunnel testing at a single point and averaged over a 3m² area. B: One roof to wall connection applied force coefficients for flexible connection and rigid connection. C: Displacement of RTWC-S3 under B loading (Morrison et al., 2012) 4

Figure 3: A) Spatial distribution of mean pressure coefficient on hip roof house of 6.7 m eave height for varying roof slope, β , and wind direction, θ , B) Area-averaged peak pressure coefficient on hip roof house of varying eave height h and roof slope, β , in worst load direction, number in panel (Gavanski et al., 2013)..... 4

Figure 4: Roof zone diagram for hip roofs with pitches between 27° and 45° and $h \leq 60$ ft (18.3 m) (ASCE 7-16, 2017)..... 5

Figure 5: External pressure coefficient versus effective wind area for hip roofs with pitches between 27° and 45° and $h \leq 60$ ft (18.3 m) (ASCE 7-16, 2017)..... 6

Figure 6: 8d-Box nail withdrawal test results (Dao & van de Lindt, 2008) 12

Figure 7: Pressure-displacement curves for fasteners under fluctuating loading (Henderson et al., 2013b) 13

Figure 8: Drone imagery of roof sheathing failures from Barrie tornado on July 15th, 2021, photo courtesy of Northern Tornadoes Project..... 17

Figure 9: Roof sheathing failure on hip roof from Barrie tornado on July 15th, 2021, photo courtesy of Northern Tornadoes Project..... 18

Figure 10: Roof sheathing failure on gable roof from Barrie tornado on July 15th, 2021, photo courtesy of Northern Tornadoes Project..... 19

Figure 11: Flow chart of experimental method.....	20
Figure 12: Finite element model of roof sheathing panel system.....	21
Figure 13: Local axis orientation for SPF truss members in the finite element model	22
Figure 14: SAP2000 frame element truss system.....	24
Figure 15: A) Sheathing panel parallel to strong axis orientation B) Sheathing panel perpendicular to strong axis orientation (Wood Handbook, 2010).....	26
Figure 16: Local axis orientation for OSB sheathing shell elements in the finite element model.....	26
Figure 17: Mesh of OSB sheathing shell elements.....	27
Figure 18: Approximate distribution and histogram of ultimate fastener capacity used in finite element model	29
Figure 19: Sample of average fastener link force-displacement curve.....	30
Figure 20: Sample of two node link.....	31
Figure 21: Grid system and link coordinates for finite element model	32
Figure 22: Trace box pressure data for fluctuating wind at 140 mph.....	34
Figure 23: Modified Time History for Finite Element Model Fluctuating Load	34
Figure 24: Layout of applied pressure for spatially-varying load case.....	36
Figure 25: Sample force-deformation behaviour from finite element model	38
Figure 26: Distributions for three load cases for a 6 in by 12 in fastening schedule.....	42
Figure 27: Distributions for three load cases for a fastening schedule of 6 in by 6 in	43
Figure 28: Distributions of three load cases for a fastening schedule of 3 in by 3 in.....	44

Figure 29: A) Geometric tributary area method for a 6 in by 12 in fastening schedule B)
Effective wind area of 9 fasteners engaged in failure for a 6 in by 12 in fastening schedule 46

Figure 30: Effective wind area method design procedure example 6 in by 8 in fastening
schedule..... 55

Nomenclature

A_A	Associated area for spatially-varying load case
A_E	Effective wind area
A_G	Geometric tributary area
A_T	Associated geometric tributary area
A_{panel}	Total area of 4 ft by 8 ft sheathing panel
C_{Fail}	Total panel force at initial failure
C_{Nails}	Mean fastener capacity
C_e	Exposure factor
$C_g C_p$	External pressure coefficient
$C_{gi} C_{pi}$	Internal pressure coefficient
C_t	Topographic factor
d_F	Shank diameter of nail
E	Modulus of Elasticity
F_{uniform}	Total panel force under uniform loading
F_{SV}	Total panel force under spatially-varying loading
f_{SV}	Spatially-varying loading factor
G	Mean relative density of main embedment material
G_{SM}	Shear modulus
GC_p	External pressure coefficient
$(GC_p)_G$	External pressure coefficient based on geometric tributary area

$(GC_p)_e$	External pressure coefficient based on effective wind area
GC_{pi}	Internal pressure coefficient
I_w	Importance factor
J_A	Toe-nail connection factor
J_B	Nail-clinching factor
K_{SF}	Service condition factor
K_T	Treatment factor
L_p	depth of penetration into main member
n_F	Number of fasteners in connection
N	Number of fasteners fully engaged in initial panel failure
P_{rw}	Nail withdrawal connection capacity
q	Wind pressure
q_G	Sheathing panel capacity using geometric tributary area
q_x	Local 1 in 50-year hourly mean windspeed
q_x	Local 1 in 50-year hourly mean windspeed
q_h	Local wind velocity pressure at mean roof height
T	Time of initial failure
v	Wind velocity
Y_w	Withdrawal resistance per millimetre of penetration
y_w	Withdrawal resistance factor

ϕ	Factor of safety
ρ	Density of air
ν	Poisson's Ratio

Chapter 1 Introduction and Background

1.1 Preface

In North America upwards of 90% of buildings are wood-frame construction, many of which are residential homes (van de Lindt & Dao, 2009). With the commonality of these structures and their sensitivity to major wind events it is of particular concern for engineers to evaluate these structures and assess their design standards. Low-rise buildings have historically been vulnerable to the effects of highspeed wind events, including tornadoes. Relatively light components and building envelope materials (e.g. roof sheathing) can be breached and cause damage such as water intrusion, or catalyze more serious structural failure. Society would greatly benefit from wind loading based improvements to wood frame structures in terms of general safety over the lifetime of the structure, and optimized design.

1.2 Wind in the Atmospheric Boundary Layer

To properly design for wind loads, the behaviour of wind needs to be understood. The characteristics of wind vary vastly depending on geographic, physical, and environmental factors. Despite these differences, many generalizations can be made about the behaviour of wind within the atmospheric boundary layer, the lowest region of the atmosphere in which most structures are immersed (Holmes, 2004). Depth of the atmospheric boundary layer varies but is typically defined as being within the first kilometre of the atmosphere extending upwards from Earth's surface. Within the boundary layer, the velocity increases logarithmically with height. The profile shape can be attributed to friction caused by conditions of the Earth's surface, for instance, deserts and oceans or suburbs and forests can be attributed to low and high degrees of friction, respectively, this variation can be seen in Figure 1 below. However, the wind velocity profile is not entirely smooth and is disrupted by turbulence, both natural and obstruction created (Davenport, 1964). Obstruction-created turbulence strongly influences the rapidly increasing part of the velocity profile which creates temporally varying loads. Quantifying this is of particular importance on all buildings.

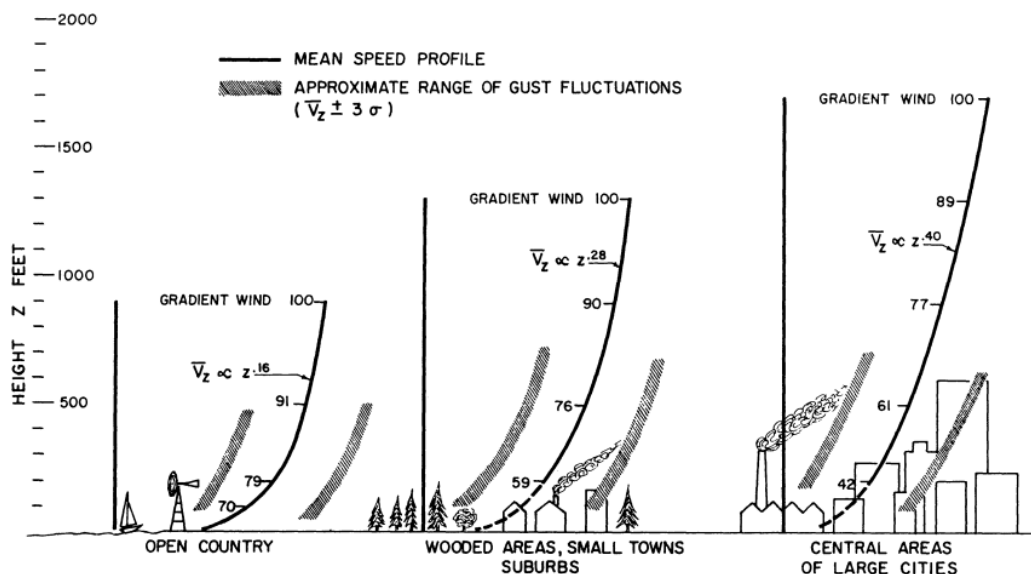


Figure 1: Mean wind velocity profile for various surface friction and terrain (Davenport, 1964)

Statistical characterization of wind is imperative to determine the effect it has on structures. It is usually assumed that the wind is statistically stationary, and it is broken down into two components: mean and fluctuating. Values used to calculate the mean and fluctuating wind components are taken from wind speed data observed at various locations, traditionally airports, and can be used only for a particular area in which data is collected. These are then used to establish values of gust wind speeds used for design.

To assess the interactions of wind profiles on specific structures requires specific investigation, usually with wind tunnels. The Boundary Layer Wind Tunnel (BLWT) at Western University focuses on the interactions of scale models and fully developed boundary layers (Gavanski et al., 2013). The Insurance Research Lab for Better Homes uses pressure loading actuators on full-scale wood-frame homes to simulate realistic wind loading the structures (Kopp et al., 2010). With facilities such as the ones mentioned above engineers can derive the exact behaviour of wind and its influence on structures of varying sizes and differing design.

1.2.1 Wind Loading on Wood-Frame Homes

Design codes such as the National Building Code of Canada (NBCC) and the American Society of Civil Engineers Standard 7-16 (ASCE 7-16) rely on research conducted at these laboratories to develop appropriate provisions for wind loads on structures. Wind tunnel test results on scale model homes shown in Morrison et al. (2012) demonstrate the high degree of variation in external wind pressure coefficients specifically on roofs, which are the most vulnerable part of the structure. These loads have significant spatial-temporal variations that create equally significant pressure variations on structure. These are shown in Figure 2 for a gable roof and Figure 3 for a hip roof, the two most common roof shapes in residential home construction. Using the BLWT at The University of Western Ontario, Gavanski et al. (2013) explored pressures on hip and gable roofs. Further investigation into spatial-temporal varying wind loads was conducted in the “3 Little Pigs” (3LP) project by Kopp et al. (2010), that conducted full-scale building tests under these loads. With these resources multitudes of researchers have been able to investigate failure of different structural components. Roof-to-wall connections have been studied by Henderson et al. (2013a) and Gavanski & Kopp (2017), while toe-nail connection performance was discussed by Morrison & Kopp (2010) and Henderson et al. (2013a) under fluctuating wind loads. Failure of batten-to-rafter connections under fluctuating wind loads were also looked at by Parackal et al. (2020) at Cyclone Testing Station. Gable roof wind loading was characterized with stochastic simulation methods by Cope et al. (2005), while the same roof shape was studied under fluctuating loads by Morrison et al. (2012). Overall wood frame roof reliability and design was also covered by Rosowsky & Cheng (1999) and Rosowsky & Qingxin (2000), respectively. Throughout all the studies above, multiple components of the overall roof structure have been examined yet individual sheathing panels have not been, even though they are a key component of the roof structure.

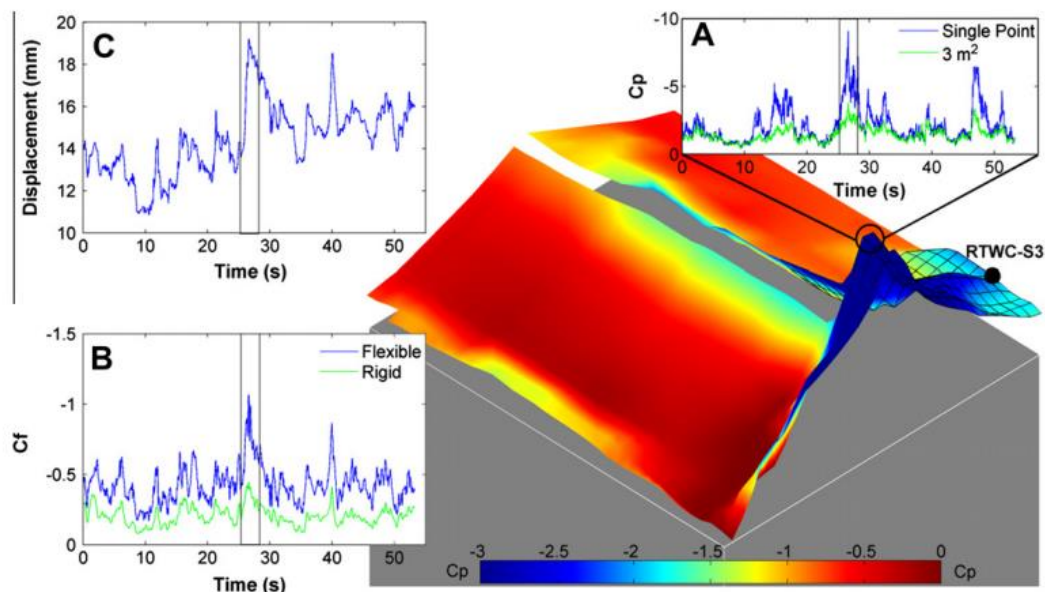


Figure 2: Spatial gradient contours for external wind pressures on the roof of the test house. A: External pressure coefficients from wind tunnel testing at a single point and averaged over a 3 m^2 area. B: One roof to wall connection applied force coefficients for flexible connection and rigid connection. C: Displacement of RTWC-S3 under B loading (Morrison et al., 2012)

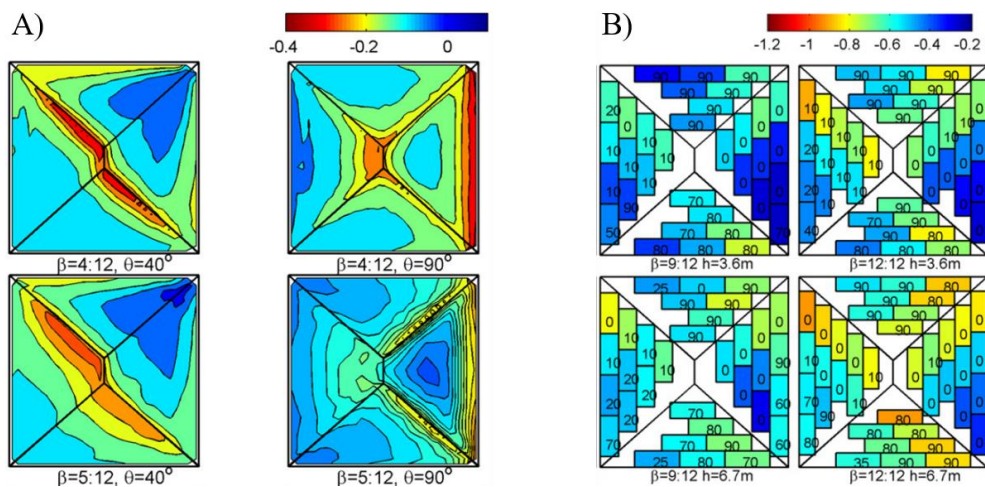


Figure 3: A) Spatial distribution of mean pressure coefficient on hip roof house of 6.7 m eave height for varying roof slope, β , and wind direction, θ , B) Area-averaged peak pressure coefficient on hip roof house of varying eave height h and roof slope, β , in worst load direction, number in panel (Gavanski et al., 2013)

Wind loads vary spatially and temporally, which can be difficult to quantify and expensive to test for every new structure. Low-rise structures fall into a category in which it is unnecessary to conduct laboratory testing for newly built structures. As a result, building codes resort to using a static loading approach for design opposed to dynamic loading. For components and cladding, ASCE 7-16 makes use of decreasing logarithmically varying plots that evaluate external pressure coefficients (GC_p) versus effective wind area on low-rise structures. ASCE 7-16 Figures 30.3-2A through 30.3-2I detail these varying external pressure coefficients for components and cladding on low-rise structures under 60 ft (18.3 m) with two general roof shapes gable and hip and several different roof pitches, varying from less than 7° to 45° , and multiple roof zones (ASCE 7-16, 2017). A sample of the ASCE 7-16 figures, specifically the one containing the most critical zone are shown in Figure 4 and Figure 5. Low-rise structure roofs are divided into several roof zones that have been identified through wind tunnel testing as regions in which the behaviour of loads is similar. These are dependent on roof shape and pitch. Within each zone, wind loading is uniform and the magnitude of the external pressure coefficient is determined by the area of the region with a minimum effective wind area of 2 to 10 sq ft. While the graphs assume a minimum zone effective wind area of 10 sq ft the increasing trend continues; however, this was not able to be seen at the original experimentation due to the lack of resolution.

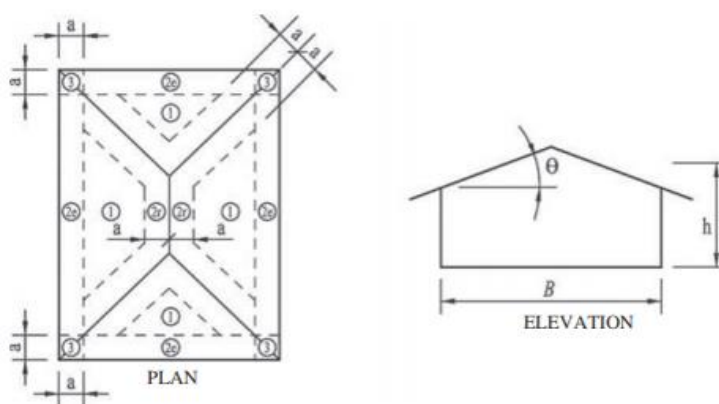


Figure 4: Roof zone diagram for hip roofs with pitches between 27° and 45° and $h \leq 60$ ft (18.3 m) (ASCE 7-16, 2017)

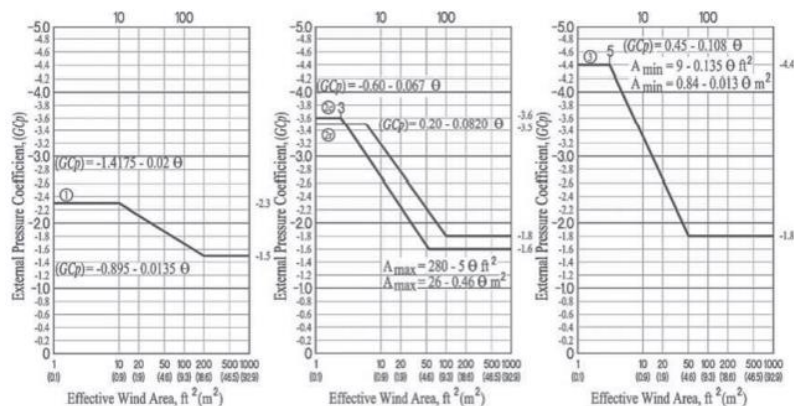


Figure 5: External pressure coefficient versus effective wind area for hip roofs with pitches between 27° and 45° and $h \leq 60$ ft (18.3 m) (ASCE 7-16, 2017)

Using the ASCE 7-16 figures, and those found in Gavanski et al. (2013), some similar regions of high magnitude pressure on the varying roof shapes and pitches can be noted. For instance, multiple figures depict a region of high negative pressure along the ridges and edge sections due to flow separation, while lower pressures occur in the central regions of the roof sections where wind loads are more constant (Gavanski et al., 2013). Thus, it can be deduced that sheathing panels in critical locations must have adequate provisions to sustain the greater wind loads.

To understand if a design is appropriate for a loading scenario, it is important to assess load paths throughout the structure. Traditionally, engineers have used a tributary area method to evaluate loading on structural elements. This assumption is conservative in that each element takes load equal to the applied load over half the span to adjacent structural elements. This fails to quantify the load sharing that occurs which could vary these values. Martin et al. (2011) and He et al. (2018) looked to quantify load sharing and determine more accurate load paths using finite element modelling throughout the entire wood-frame structure. The primary load path for forces in the main wind force resisting system is based on the path of greatest stiffness; however, because of the indeterminate nature and redundancy in the wood-frame structural system it is difficult to assess the direct load paths (He et al., 2018).

1.2.2 Wind Loading on Sheathing

Though it is critical in wood-frame construction, sheathing is not considered part of the main wind resisting system. Rather, it is considered under components and cladding and provides shear resistance and helps to keep water out. As a result, it has been closely studied under multiple different conditions. While assessing pressures on the overall roof, Gavanski et al. (2013) determined the average pressure acting on individual sheathing panels by averaging the pressure over 3 m², the size of typical sheathing panels. Miller et al. (2017) used pressure loading actuators to simulate wind loads on air-permeable cladding systems. Wall sheathing performance was assessed by Kopp & Gavanski (2012) to determine the effects of pressure equalization. Henderson et al. (2013b) investigated failure mechanisms and capacity of roof sheathing under fluctuating loads for several different fastener types and fastening schedules. Details of this experimental set up and results will be discussed further in sections pertaining to sheathing fastener behaviour and roof sheathing capacity. Assessment of roof sheathing performance is critical for determining whether current precautions are appropriate. Fragility assessment of roof sheathing and development of fragility curves has been discussed by Lee & Rosowsky (2005) and Gill et al. (2021). Reliability analysis of sheathing by Gavanski et al. (2014) determined that the current NBCC minimum intermediate truss fastening schedule for sheathing was inadequate for parts of Canada.

Current building code practices for determination of wind loading on components and cladding use effective wind area to determine the external pressure coefficient. Obtained values are then inserted into equation 30.3-1 from ASCE 7-16 (Eq (1)) for low-rise buildings components and cladding to assess the applied pressure (2017):

$$p = q_h[(GC_p) - (GC_{pi})] \quad (1)$$

where q_h is the local wind velocity pressure at mean roof height as defined in ASCE 7-16 Section 26.10 and GC_{pi} the internal pressure coefficient from ASCE 7-16 Table 26.13-1 (ASCE 7-16, 2017). Similarly, in NBCC, wind pressure coefficients are taken from Figure 4.1.7.6.-C and Figure 4.1.7.6.-E for $C_g C_p$, while C_{gi} can be taken from 4.1.7.3 Sentence (10) and Table 4.1.7.7. for C_{pi} values. The wind load is determined by

combining NBCC equations for external and internal loading, 4.1.7.3. Sentence (1) and Sentence (3) (Eq (2)), respectively:

$$p = I_w q C_e C_t (C_g C_p + C_{gi} C_{pi}) \quad (2)$$

where I_w is the importance factor for the structure, q is the local 1 in 50-year hourly mean windspeed, C_e is the exposure factor determined by the height of the structure, and C_t is the topographic factor based on the structure's surroundings (NBCC, 2015). The calculated values are then used to determine sheathing panel thickness and fastening schedules.

Similar to the entire wood-frame structure, understanding localized load paths is equally important to the design of a structure. Under wind load, sheathing is loaded 2-dimensionally, which poses a complex issue of load distribution. Load transfer paths for sheathing although less redundant than the entire structure, vary depending on loading. Current design practice does not consider load sharing amongst fasteners (nails) and uses the geometric tributary area assumption which tends to be conservative.

1.3 Sheathing Fasteners

An integral part to the strength of wood-frame structures are the fasteners. Fasteners are the path of load transfer between sheathing and lumber components. Multiple types are considered acceptable fasteners for wood-frame construction including common wire nails, common spiral nails, staples, and adhesives (AWC NDS, 2015). Although a variety are accepted in wood-frame construction, different kinds of fasteners exhibit different behaviours.

1.3.1 Design Specifications for Sheathing Fasteners

In North America common spiral or common steel wire nails are conventionally the fastener of choice and are the default fasteners in NBCC Section 9.23.3.1. (NBCC, 2015). To ensure all fasteners used in wood-frame structures are of adequate quality, they must conform to ASTM F 1667 "Driven Fasteners: Nails, Spikes, and Staples" (2021) and CSA B111 "Wire Nails, Spikes and Staples" (2003) which detail specifications for nail

material, shank depth and diameter, head diameter, and acceptable coatings. Details for the above parameters also vary based on the method of embedment either hand driven or power-tool driven (ASTM F 1667, 2021). For instance, 8d box nails made with carbon steel, stainless steel, or aluminum wire have a length of 2 ½ in (63.5 mm), diameter of 0.113 in (2.9 mm), and head diameter of 0.297 in (7.5 mm). ASTM also covers testing methods of fastener mechanical properties including dimensional, bending, hardness, coating weight and adherence tests in ASTM F 680 “Test Methods for Nails” (2020), ASTM F 1575 “Test Methods for Determining Bending Yield Moment of Nails” (2017), and ASTM F 3359 “Test Methods for Determining Yield Moment of Staples” (2019). Tensile strength of nails is the tensile strength of the material, which can be acquired using ASTM A 370 “Test Methods and Definitions for Mechanical Testing of Steel Products” (2020) methods. NBCC Table 9.23.3.1. defines minimum diameter and length of fasteners with a minimum of 2.87 mm and 57 mm, respectively (NBCC, 2015). Based on ASTM F 1667, 8d fasteners meet the minimum requirements set out in NBCC and are the minimum referenced fastener in Table 3.10 of American Wood Council’s (AWC) Wood Frame Construction Manual (WFCM) (2015).

Fastening schedules for wood-frame roofs can vary drastically depending on the area the structure is built. NBCC Section 9.23.3. details wood-frame construction fastener requirements including nail dimensions, minimum embedment depth, and maximum allowable fastening schedules. The minimum requirements for fastening sheathing in both NBCC (2015) (Tables 9.23.3.5A – 9.23.3.5C) and AWC’s WFCM (2015) (Table 3.10) assume a maximum nail spacing of 6 in (150 mm) on centre for exterior trusses and 12 in (300 mm) on centre for interior trusses, using 8d common nails. This method of determining fastener spacing assumes each fastener is independent and takes load equal to its corresponding geometric tributary area, which covers the area enclosed by half the span to adjacent fasteners. This assumption is inherently conservative given the semi-rigid properties of sheathing; thus, further exploration to quantify fastener group action is integral to reduce conservatism.

1.3.2 Capacity of Sheathing Fastener Connections

Determination of individual fastener capacity is complex and a function of several variables including mechanical and physical properties, as well as embedment material properties, and embedment orientation properties. The variation of embedment orientation properties between nearby fasteners indicates that fastener capacity is similar, but independent. However, when assessing connections, standards reduce embedment orientation properties to only simulate penetration depth and use factors of safety to accommodate the rest of the situational properties. Canadian Standards Association (CSA) O86 (2014) estimates nail withdrawal connection capacity (P_{rw}) using the following equation from CSA Section 12.9.5.2:

$$P_{rw} = \phi Y_w L_p n_F J_A J_B \quad (3)$$

where ϕ is 0.6, L_p is depth of penetration into main member, n_F represents number of fasteners, J_A represents a factor for consideration in toe-nail connections, else it is 1.0, J_B is a nail-clinching factor, and Y_w is withdrawal resistance per millimetre of penetration calculated using:

$$Y_w = y_w K_{SF} K_T \quad (4)$$

where K_{SF} represents the service condition factor in Table 12.2.1.5 of CSA O86, K_T is the treatment factor found in CSA Clause 4.3.2 and y_w is equal to:

$$y_w = 16.4 d_F^{0.82} G^{2.2} \quad (5)$$

where d_F is the shank diameter and G is the mean relative density (CSA O86, 2014). For a single 8d box nail used to fasten $7/16$ in (11.1 mm) thick oriented strand board (OSB) sheathing to a 2 x 4 Spruce Pine Fir (SPF) truss member would have an estimated withdrawal capacity using equation (3) of 183 N. Where the mean relative density of SPF is 0.42, while the lumber service condition factor (K_{SF}) and treatment factor (K_T) are 1 for dry lumber and nails under withdrawal loads and untreated lumber, respectively (CSA O86, 2014). While a diameter of 2.9 mm and penetration into main member is 52.4 mm (8d nail length less depth of sheathing) is used (CSA O86, 2014). With toe-nailing factor

(J_A) and nail-clinching factor (J_B) equal to 1.0 for not being a toe-nail connection and not clinched nails, respectively (CSA O86, 2014). The calculated estimate of capacity is then used to determine fastening schedules for a roof such that it meets the components and cladding force governed by equations (1) or (2), depending on the jurisdiction. Values calculated using estimation equations found in standards include safety factors so that designs are conservative.

Withdrawal tests to determine wood-fastened connection capacities are paramount in assessing if connection assumptions are accurate. Test methods prescribed by ASTM D 1761 “Tests for Mechanical Fasteners in Wood” (2021) ensure adequate withdrawal and lateral resistance. Following these methods, Dao & van de Lindt (2008) collected withdrawal and bending force-displacement data from 10 specimens with the maximum average load being 688 N and a displacement of 4 mm. The withdrawal behaviour of this test can be seen in Figure 6 and will be discussed further in the Section 2.1.3. The test specimens used 8d box nails fastened through 12 mm thick OSB sheathing attached to a 2 x 4 (38 x 89 mm). Dao & van de Lindt (2008) used these results to create a more accurate finite element model for fasteners under varying suction (withdrawal) loads. The model was subjected to an incremental uniform load to a maximum of 7.2 kPa, a load at which certain failure would occur. The critical fastener modelled using the coupled results of withdrawal and bending tests had a maximum displacement of 34 mm. These values will be discussed further under model definition of links in Section 2.1.3. Fastener capacity was found to have a Gaussian distribution by Murphy et al (1996). Rosowsky & Schiff (1999) also conducted testing to determine the impact that combined lateral and withdrawal loads had on sheathing fasteners. Tests examined both 8d common and ring shank nails, No. 8 screws, and polyurethane adhesive between $^{15}/_{32}$ in 3-, 4-ply plywood or $1/2$ in OSB sheathing and SPF or southern yellow pine (SYP) 2 x 4 lumber, under varying angles to induce combined withdrawal and lateral loading (Rosowsky & Schiff, 1999). Withdrawal capacities of nail fasteners under pure withdrawal load varied between 422 N (95 lb) for the instance of hand driven 8d common nail in $1/2$ in OSB sheathing and SPF 2 x 4 lumber, and 1543 N (347 lb) for the instance of hand driven 8d common nails in $^{15}/_{32}$ in 4-ply CDX plywood and SYP 2 x 4 lumber (Rosowsky & Schiff, 1999). The

discrepancies between tested fastener capacity and calculated design capacity result in large factors of safety.

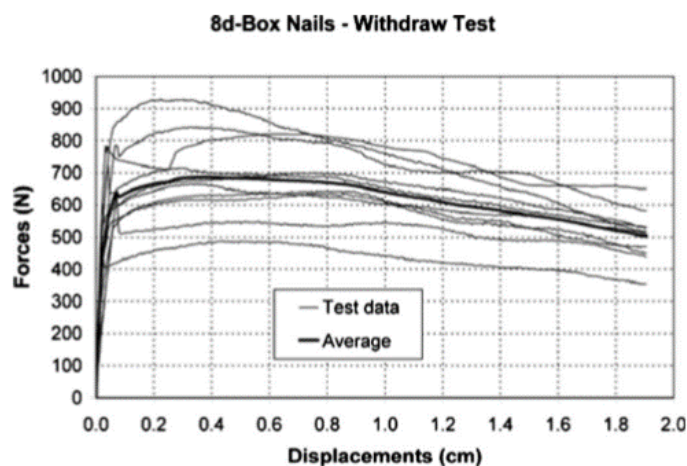


Figure 6: 8d-Box nail withdrawal test results (Dao & van de Lindt, 2008)

1.3.3 Behaviour of Sheathing Fasteners under Wind Loading

Roof sheathing fasteners are integral to the strength of the roof system. As such, it is imperative to understand their behaviour under negative pressure, suction, which causes withdrawal. A lack of loading perpendicular to the withdrawal direction indicates that shear strength and deformation are negligible under wind loading on the roof. Henderson et al. (2013b) collected data at fastener locations during testing of sheathing panels under fluctuating loading. Notably, fastener withdrawal followed damaging peaks of the fluctuating loading, incrementally increasing as damaging peaks occurred. This incremental failure of fasteners was also seen in other experiments including Morrison & Kopp's (2011) study of toe-nail connections and Kopp & Gavanski's (2012) study of wall sheathing system performance under fluctuating loads. Peak force-deformation points from Henderson et al. (2013b) shown in Figure 7 form a 'backbone' curve resembling steel stress-strain diagrams. Dao & van de Lindt's (2008) force-deformation curves from experiments (Figure 6) are similar in shape to the 'backbone' curves of Henderson et al. (2013) (Figure 7). The curves have 3 distinct ranges: elastic, plastic, and softening. The elastic range exhibits a linearly proportional relationship between the applied force and the deformation, and when unloaded the fastener will follow the curve

with no permanent deformations. After pushing past the fasteners yield capacity the relationship between force and deformation has a smaller slope, with larger, permanent deformations. Unloading the fastener in this section causes the fastener to begin receding from its maximum deformation point following the elastic slope, parallel to the initial elastic range. During reloading the deformation will follow the parallel elastic curve and continue plastic deformation as load increases. Once the fastener reaches its ultimate capacity it enters the softening range and can take no additional force but will continue to deform, indicating that the fastener no longer contributes to the stability of the panel and has failed. Henderson et al. (2013b) noted two failure types: fastener pull out, where the shank was removed from the truss element, and fastener pull through, where the fastener head pulled through the sheathing. Fastener pull out is more common for the fasteners examined. Fastener head diameter was observed to impact the likelihood of pull through failure behaviour (Henderson et al., 2013b). Discussion of the contributions of individual nail failure and its impact on the system will be discussed in the sheathing failure section of this thesis.

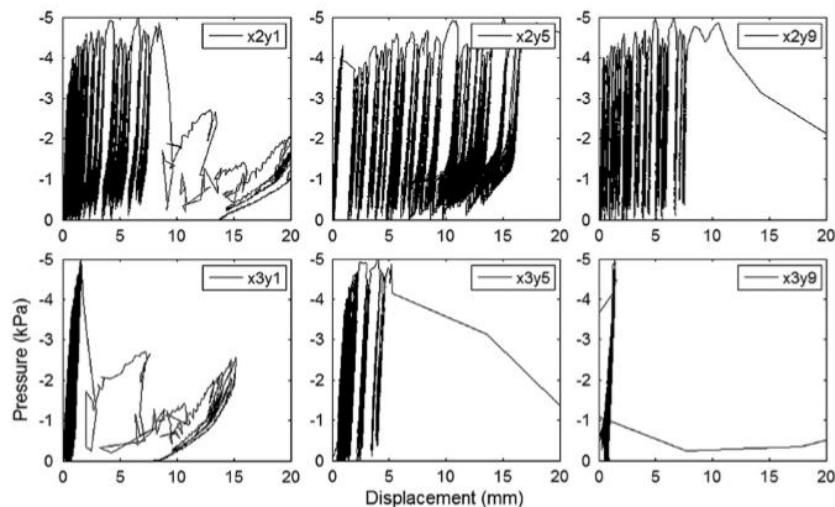


Figure 7: Pressure-displacement curves for fasteners under fluctuating loading (Henderson et al., 2013b)

1.3.4 Rate of Loading Impacts on Sheathing Fasteners

Determination of behaviour and failure mechanisms of fasteners under varying load conditions is imperative for design. Quantifying the impacts for varying load durations and the rate at which it was applied is paramount. Rosowsky & Reinhold (1999) investigated these effects to determine the impact, if any, of both circumstances. Using both withdrawal and lateral load testing with 8d common nails and No. 8 screws in SPF 2 x 4 (38 x 89 mm) lumber (Rosowsky & Schiff, 1999). A displacement control method, where the displacement is altered and other variables are noted, was used and it was determined under both withdrawal and lateral load testing that the rate at which load is applied does not impact the behaviour mechanisms of the fasteners (Rosowsky & Schiff, 1999).

1.4 Roof Sheathing

Sheathing is a thin flexible wood panel that is used in wood-frame construction for a variety of components including exterior walls, floors, and roofing. As a material with such diverse uses, it must meet requirements for a main structural member and cladding. Various sheathing types are acceptable including oriented strand board (OSB), plywood, and waferboard, with numerous different materials (NBCC, 2015). These specimens must meet rigorous standards to ensure appropriate performance.

1.4.1 Design Specifications for Roof Sheathing Panels

Sheathing selection for wood-frame roofs differs from sheathing used in flooring or walls. Roof sheathing falls under cladding and does not contribute to the main lateral load support system of the structure (NBCC, 2015). As such axially loading capacity or loading through the thickness of the sheathing is negligible, but out of plane bending capacity is critical. Several Canadian standards govern dimensions and capacities of roof sheathing depending on the material and type of sheathing including CSA O121 “Douglas Fir Plywood” (2017), CSA O151 “Canadian Softwood Plywood” (2017), CSA O153 “Poplar Plywood” (2019), CSA O325 “Construction Sheathing” (2021) and CSA O437.0 “OSB and Waferboard” (2011) (NBCC 2015, 2015). Other standards such as ASTM D 3043 “Test Methods for Structural Panels in Flexure” (2017) and ASTM D

7033 “Establishing Design Capacities of Oriented Strand Board (OSB) Wood Based Structural-Use Panels” (2014), detail testing set ups and design guidelines. Typical sheathing panels are 8 ft by 4 ft in size but vary in depth depending on truss spacing and loading. NBCC Table 9.23.16.7.-A specifies minimum roof sheathing thickness based on truss spacing, edge support, and type of sheathing (NBCC, 2015). For instance, the minimum thickness of O-1 grade OSB sheathing at 600 mm truss spacing is 11.1 mm ($7/16$ in) thick (NBCC, 2015). Sheathing panel size can also be determined from loads and required capacity, especially in regions susceptible to major windstorms.

1.4.2 Capacities of Roof Sheathing Panels

Capacity of roof sheathing refers to the amount of force the panel can take in flexure (ASTM D 7033, 2014). To determine this value a fastened sheathing panel is uniformly loaded and subjected to a linearly increasing load; however, this does not reflect actual loading (Henderson et al., 2013b). CSA O86 and CSA O325 do not provide methods for calculating a value for specific sheathing capacity but detail strength, stiffness, and rigidity capacities per nominal thickness of Douglas fir plywood, Canadian softwood plywood, and OSB sheathing panels to fit calculated design needs (CSA O86, 2014).

Several experiments have been conducted to determine the capacity of roof sheathing including Sutt (2000) and Henderson et al. (2013b). Henderson et al. (2013b) evaluated the capacity of sheathing using different fasteners including twist and ring shank, hurricane, coated ring-shank nails and staples. The panels were then subjected to a 0.32 kPa/sec uniform ramping load with mean $7/16$ in OSB sheathing capacities varying from 4.00 kPa to 5.79 kPa for twist shank nails and staples, respectively (Henderson et al., 2013b). The same fasteners were also subject to fluctuating loads which followed several 900 second connected segments of fluctuating pressure used in Kopp & Gavanski (2012) with pressure results of $7/16$ in OSB sheathing varying between 4.06 kPa and 5.39 kPa for twist shank nails and hurricane nails, respectively (Henderson et al., 2013b). From this study it was determined that failure capacities under ramp loading were similar enough to the fluctuating loads that they accurately reflected sheathing capacity (Henderson et al., 2013b). While Sutt (2000) investigated the interactions of normal and shear loading interaction. Pure normal loading of $7/16$ in OSB sheathing resulted in capacity values

varying from 2.39 kPa (50 lbs/ sq ft) to 3.83 kPa (80 lbs/sq ft) (Sutt, 2000). Capacity of sheathing panels is highly dependent on the material and thickness of the panel, however, behaviour under loading is similar between laboratory experiments and in the field.

1.4.3 Failure of Roof Sheathing Panel Systems

Understanding the method in which a connection or member fails allows engineers to develop adequate design provisions to mitigate the failure. The definition of failure from an engineering position varies from what can be perceived as failure. Engineering failures typically define failure as the point in which failure is initiated or one component has failed, whereas perceived failure indicates total failure of the part or structure.

Engineering failure in reference to sheathing panels would indicate a fastener has failed, while perceived failure would be failure of all fasteners and removal of a sheathing panel. Studying behaviours of sheathing failures in both a laboratory setting and on site of major wind events aids are both paramount for appropriate design.

Testing on individual sheathing panels under uplift loading conditions to determine failure capacity by Henderson et al. (2013b) detailed the failure mechanism. The failure condition was defined as all fasteners had been withdrawn from the trusses. It was noted failure initiated at fasteners located along the central 3 trusses, at the internal location, which then spread to adjacent fasteners along the same truss and on neighbouring trusses. Initial failure started an ‘unzipping’ effect that resulted in total failure occurring shortly after initial failure (Henderson et al., 2013b). This failure mechanism shows that both failure types are similar and that roof sheathing engineering failures are a good representation of overall panel performance.

Damage surveys found that roofs are susceptible to roof sheathing occurrences and this failure method is of particular importance due to its impact on losses (Gavanski et al., 2014). In field surveys done after tornado events in Canada detail failures of wood-frame structures, known as degree of damage (DODs), which are then used to assess the severity of the event (Morrison et al., 2014). Failure of roof sheathing from severe wind events involves the total removal of whole sheathing panels as shown below (Kopp et al., 2017 & Morrison et al., 2014). These images show that removed panels can become

windborne, causing additional damage to surrounding structures. Further highlighting the importance to study the independent system of the sheathing panel to improve design provisions.



Figure 8: Drone imagery of roof sheathing failures from Barrie tornado on July 15th, 2021, photo courtesy of Northern Tornadoes Project



Figure 9: Roof sheathing failure on hip roof from Barrie tornado on July 15th, 2021, photo courtesy of Northern Tornadoes Project



Figure 10: Roof sheathing failure on gable roof from Barrie tornado on July 15th, 2021, photo courtesy of Northern Tornadoes Project

1.5 Objectives

Current design of roof sheathing systems indicate fastener capacities are to be considered independent. However, based on prior studies it was noted that given the spacing between fasteners and the limited flexibility of the panel it is not probable that fasteners could fail independently without incorporating strength from neighbouring fasteners. Failure progression of the panel also indicates that after failure of one fastener, neighbouring fasteners fail soon after indicating an increase in burden due to the prior failure. Thus, the hypothesis for the current study is that load sharing among fasteners is important to include when evaluating overall panel capacity. The objective of this thesis is to develop a method to determine effective wind area and apply the method to determine effective wind area of roof sheathing panel systems under realistic uplift wind pressures.

Chapter 2 Methodology

The methodology for determining the effective wind area of sheathing is discussed in this chapter. To predict the behaviour of the sheathing system including fastener forces and deformations under differing uplift wind cases and identifying the corresponding effective wind areas, the finite element method, a powerful numerical tool is used. The finite element model is then integrated with a Monte Carlo simulation to consider the boundary conditions, element properties, and loading situations, to determine the effective wind area from force and deformation outputs. Checks are then performed on the model results to ensure model stability and validity. A flow chart of the experimental method is shown below in Figure 11.

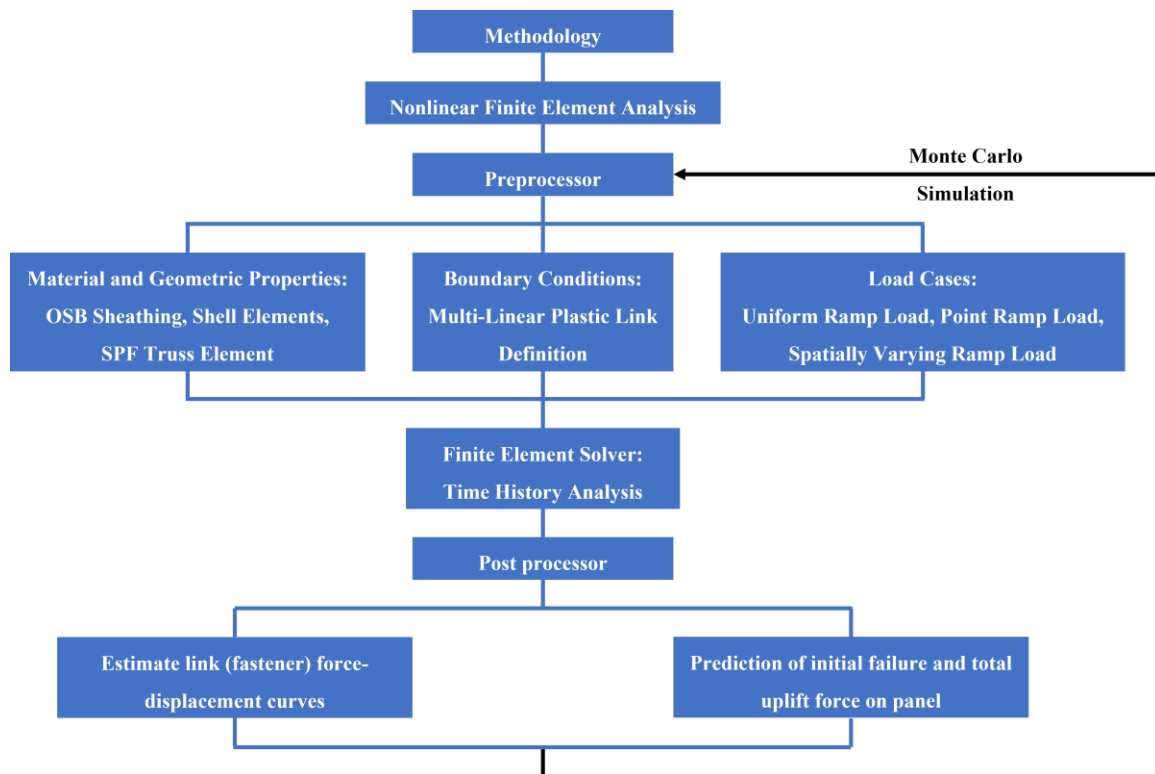


Figure 11: Flow chart of experimental method

2.1 Finite Element Model

Determination of effective wind area for roof sheathing requires analysis of individual sheathing panels. This behaviour can be studied using finite element analysis software

where data is able to be collected at small intervals at multiple defined locations. A single sheathing panel system is modelled including truss members, fasteners, and sheathing that replicate typical construction and can be seen in Figure 12. SAP2000 was selected as the analysis software.

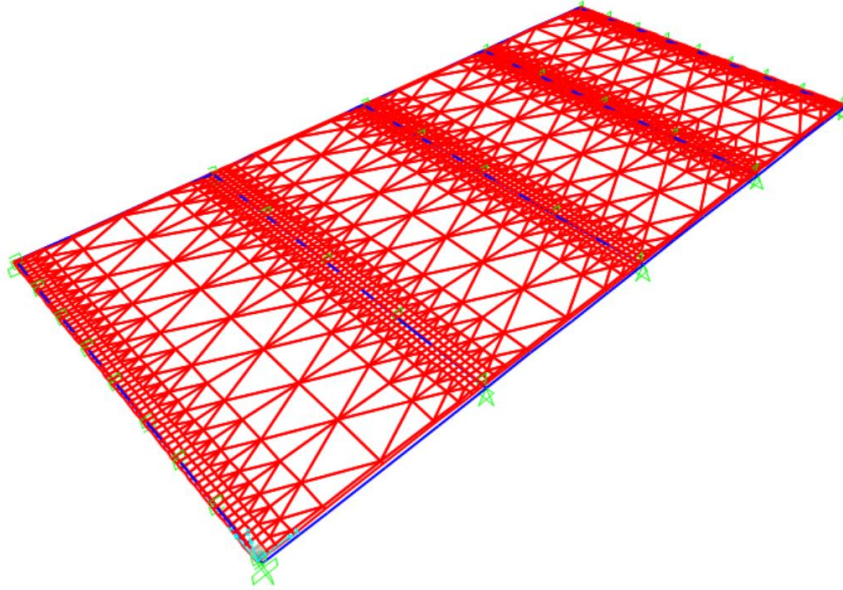


Figure 12: Finite element model of roof sheathing panel system

2.1.1 SPF Trusses Using Orthotropic Frame Elements

To simulate the bending rigidity of the roof sheathing system, roof truss members should be considered in the model. Bending rigidity of the truss-sheathing system significantly affects sheathing deformation and accordingly the load sharing between the fasteners. Typical 2 x 4 (38 x 90 mm) SPF trusses were modelled as frame elements with rectangular cross sections. Orthotropic material properties are defined to simulate the difference in bending rigidity of lumber in the model.

Wood members are unique in that their properties vary depending on the axis unlike other isotropic materials. To capture this phenomenon, the truss member material is defined as orthotropic to individually assign moduli of elasticity, Poisson's ratio, and shear moduli to their corresponding axis. The United States Department of Agriculture (USDA) Wood Handbook (2010) Tables 5-1, 5-2, and 5-3a, CSA O86 (2014) Table 6.3.1A, and the

American Wood Council (AWC) National Design Specifications (NDS) Supplement (2018) Table 4-B provide reference design values for the material properties of varying size and material. The defined properties include modulus of elasticity, bending strength, ratios between axis modulus of elasticity, Poisson's ratio, and specific gravity. Material properties for SPF truss members found in Table 1, were set assuming the truss member is comprised of southern pine No. 2, with modulus of elasticity and strength values from Table 4B of NDS Supplement (2018), and Poisson's ratio from USDA Wood Handbook (2010) Table 5-2. The specific gravity specified in NDS Supplement (2018) Table 4B, corresponding to a mass per unit volume of 581 kg/m^3 and force per unit volume 5700 N/m^3 was then applied to the frame element. Properties were assigned based on local axis definition as shown in Figure 13. Material properties were then linked to a defined 2 x 4 (38 x 89 mm) width (w) and height (h), respectively, rectangular cross section and visually inspected for correct orientation after being drawn.

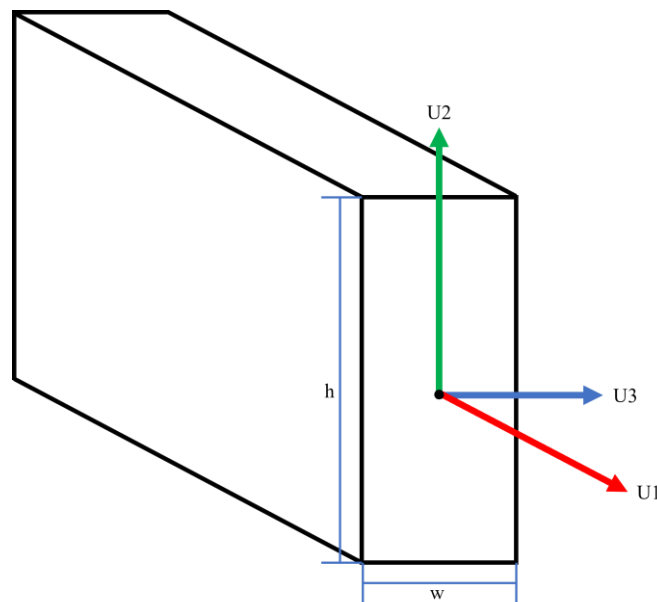


Figure 13: Local axis orientation for SPF truss members in the finite element model

Table 1: SPF Truss Orthotropic Frame Element Material Property Data

	Axis		
	U1	U2	U3
Modulus of Elasticity (Pa)	9.65 (10 ⁹)	5.73(10 ⁸)	9.30(10 ⁸)
Poisson's Ratio	0.361	0.345	0.364
Shear Modulus (Pa)	6.24(10 ⁸)	6.69(10 ⁸)	1.12(10 ⁸)

Wood-frame roof truss spacing can vary based on geographic location and support needs of the structure. In the AWC WFCM Table 3.10 lists fastening schedules for typical roof truss spacing including 12 in, 16 in, 19.2 in, and 24 in. Similarly, the Canadian Wood-Frame House Construction manual (2014) uses roof truss spacing of 16 in and 24 in, as listed in Table 34. For the current model, the common 24 in (610 mm) on centre truss spacing is selected, with connecting members along the edges. The centroid of the truss frame element is inserted at -5 mm along the z-axis; this value was arbitrarily selected for fastener length and will be discussed further in Section 2.1.3. Pinned boundary conditions are applied at the end of the trusses that restrict translation in all directions while allowing rotation, truss connections were not being studied, thus, it was determined this simplification was acceptable. Figure 14 shows a plan view of the panel trusses with labels A through E, from left to right.

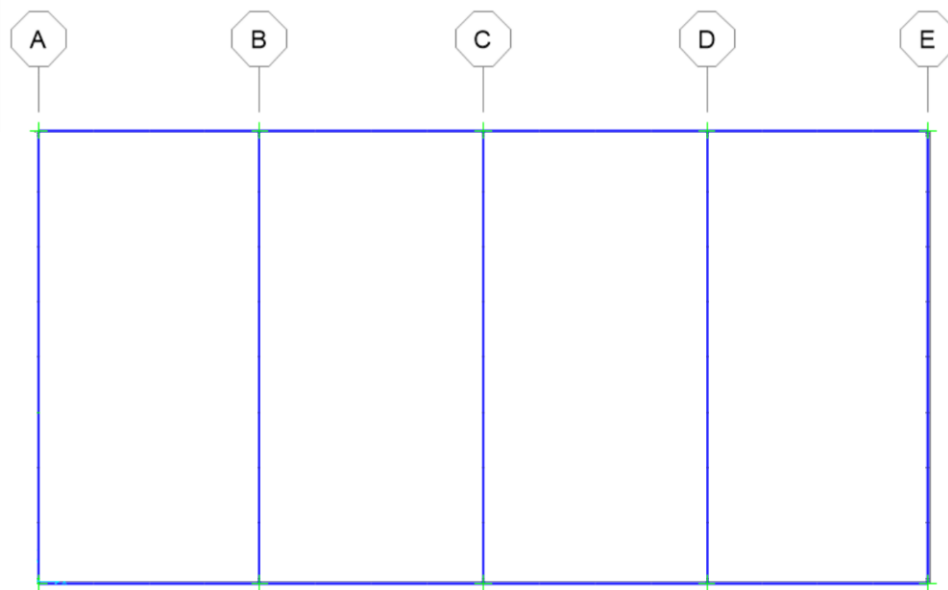


Figure 14: SAP2000 frame element truss system

2.1.2 OSB Sheathing Using Orthotropic, Thin Shell Elements

Similar to truss elements, modelling of sheathing is unique given the variety of properties for different orientations. The smallest allowable sheathing thickness is $\frac{7}{16}$ in (11.1 mm) for OSB panels, which is selected for analysis, similar to those used by Henderson et al. (2013b). As the depth of the panel is relatively thin compared to other dimensions of the panel a thin shell element with orthotropic material properties is selected.

To determine the orthotropic properties of $\frac{7}{16}$ in OSB sheathing, multiple sources were consulted. The USDA Wood Handbook (2010) defines mechanical properties of wood-based composite materials including plywood and OSB sheathing. Table 12-3 provides the results for the modulus of elasticity both parallel and perpendicular to the strong axis, as shown in Figure 15 below. The modulus of rupture, internal bond strength, and specific gravity for 3 different wood species of OSB sheathing were taken from 3 experiments, Biblis (1989), Pu, et al. (1992) and Wang, et al. (2003) (Wood Handbook, 2010). Modulus of elasticity values varied between 4.41 GPa and 7.90 GPa with an average of 5.70 GPa parallel to the strong axis and 1.40 GPa to 3.17 GPa with an average of 2.43 GPa perpendicular to the strong axis (Wood Handbook, 2010). The average values were used to model the OSB sheathing. OSB sheathing, as a composite material,

does not have a predefined Poisson's ratio. Thomas (2003) investigated the Poisson's ratio of multiple sheathing panels of varying thickness from 17.17 mm to 19.23 mm with an average of 18.35 mm along both parallel and perpendicular to the strong axis. The parallel to strong axis Poisson's ratio was determined to be 0.226 with a coefficient of variation of 0.212 while perpendicular to the strong axis ratio was 0.159 with a coefficient of variation of 0.145 (Thomas, 2003). These values were then used to calculate the shear modulus, using the conversion equation:

$$G_{SM} = E/2(1+\nu) \quad (6)$$

where E is the modulus of elasticity and ν is the Poisson's ratio for the axis. The sheathing panel is modelled using a shell element which considers both bending and membrane rigidities. Since no loads are applied in the sheathing plane and the wind uplift acts perpendicular to the sheathing, only shell bending stiffness is considered in the analysis. As such, the membrane rigidity is set to zero which has no impact on results. Properties were assigned according to the local axis number as depicted in Figure 16 and listed in Table 2 and applied to the thin shell element. Bending depth of the shell element was equal to 11.1 mm, the depth of the entire panel, to represent the thin and flexible nature of the panel. Shell elements were developed for at a typical panel size of 4 ft by 8 ft.

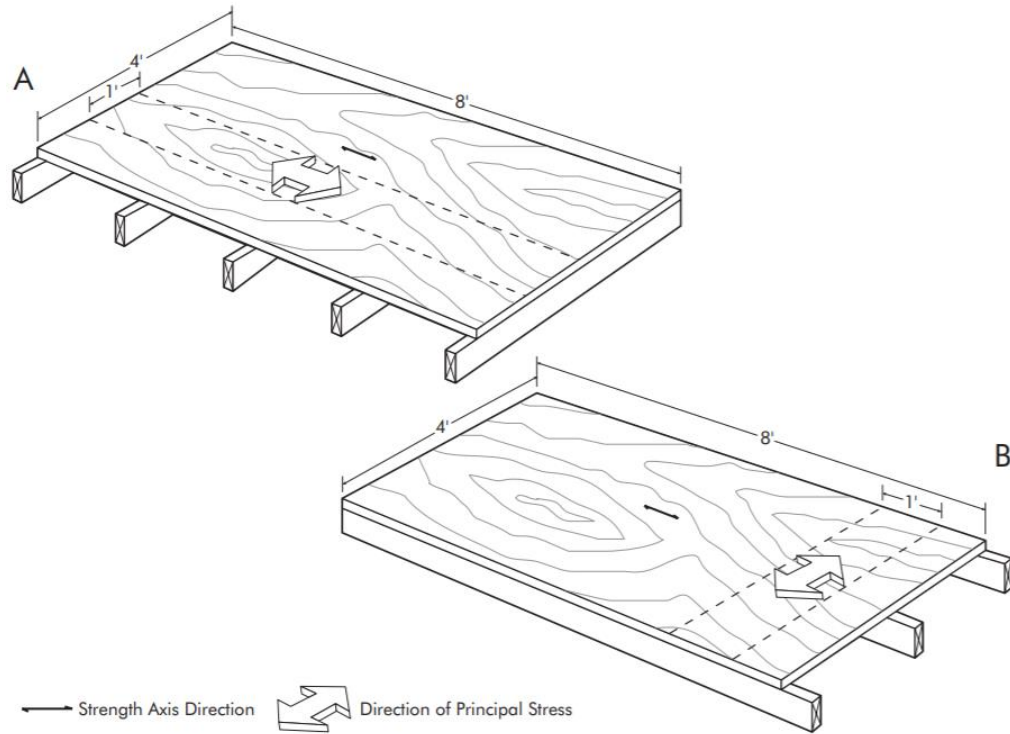


Figure 15: A) Sheathing panel parallel to strong axis orientation B) Sheathing panel perpendicular to strong axis orientation (Wood Handbook, 2010)

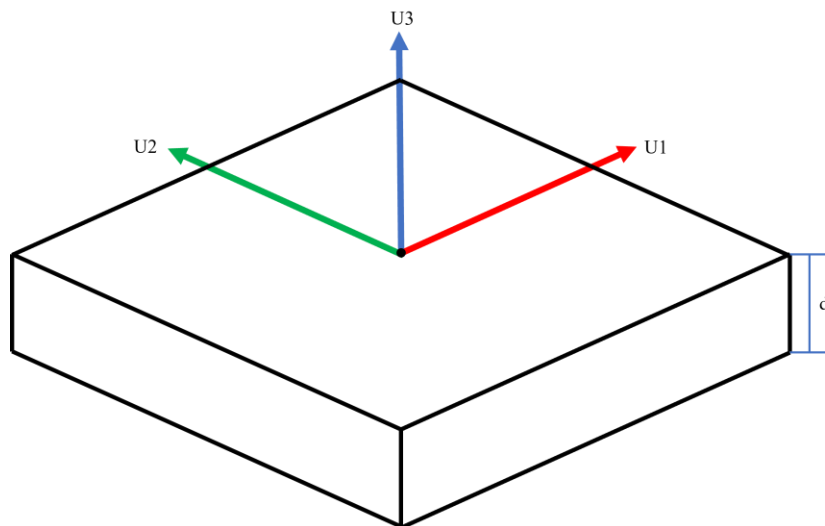
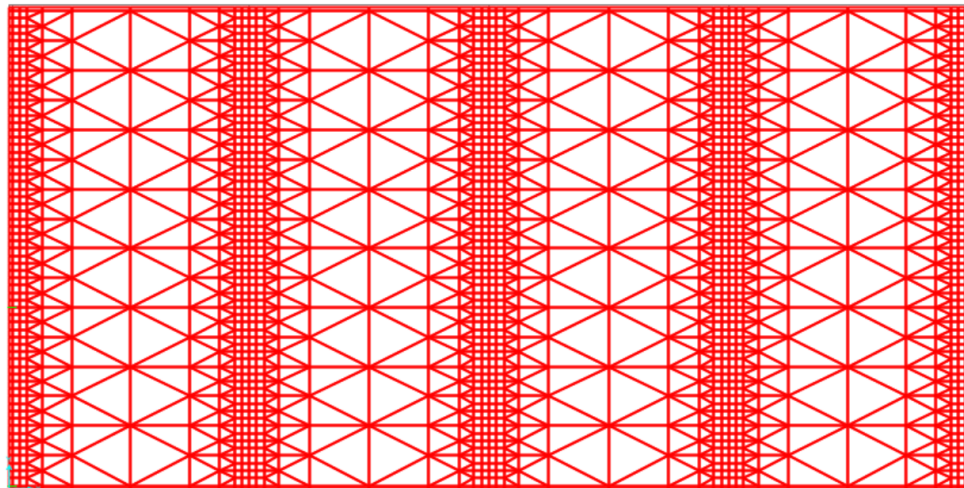


Figure 16: Local axis orientation for OSB sheathing shell elements in the finite element model

Table 2: OSB Sheathing Shell Element Orthotropic Property Data

	Axis		
	U1	U2	U3
Modulus of Elasticity (Pa)	5.7(10 ⁹)	2.43(10 ⁹)	0
Poisson's Ratio	0.226	0.159	0
Shear Modulus (Pa)	2.32(10 ⁹)	1.05(10 ⁹)	0

The sheathing panel is discretized into number of shell elements, which is called a finite element mesh. A combination of triangular and rectangular elements is used to have the mesh grading shown in Figure 17. Two types of strips can be defined in the sheathing panel: fastener strip at the location of the trusses and a middle strip where the sheathing panel extends between two trusses. Finer mesh with smaller size elements of 20 mm square sections define the fastener strip, while large triangular elements represent the middle strip. An aspect ratio, the ratio of longest to shortest dimension, is kept under 3, in agreement with typical modelling practice. The shell elements were drawn with a centroid insertion point in the x-y plane.

**Figure 17: Mesh of OSB sheathing shell elements**

2.1.3 Fasteners Using Two Node, Multi-Linear Plastic Links

Behaviour of mechanical fasteners is paramount to ensure accurate sheathing failure capacities. As seen in Figures 5 and 6 above, under direct withdrawal, the fasteners exhibit a linear elastic range, a hardening phase, and a softening phase, while under fluctuating loading these same phases are exhibited but with plastic deformations. To replicate this behaviour a multi-linear plastic link was selected such that a multi-linear model for the elastic and plastic ranges could be defined. As well as softening after failure, some modifications were made due to program constraints, which will be detailed below.

Mechanical properties of fasteners are innately complex due to the situational dependent factors involved. Specific characteristics like embedment angle and depth are difficult to quantify; thus, for simplification the variation of these factors is not considered in the model. Multiple failure mechanisms are also plausible for mechanical fasteners; however, only pull-out behaviour and failure type are investigated in this thesis. Multi-linear plastic link definition require several points be used to construct a hysteresis loop. The loop is defined by several points including the yield, ultimate, plateau, and softening points. Isotropic hysteresis is selected since the unloading is parallel to the initial stiffness which matches behaviour noticed in physical experiments. Furthermore, other hysteresis types while unloading follow a more complex nonlinear relationship which might cause numerical instability. The isotropic hysteresis type also provides better convergence and numerical stability for nonlinear analysis under uplift fluctuating and ramping loading. Withdrawal tests on 8d box nail samples by Dao & van de Lindt (2008) were used to determine values for modelling fasteners of which the average ultimate capacity was 688 N at 4 mm (Figure 6). It was found that when placed under a failure load, the maximum deformation of the coupled links is about 34 mm (Dao & van de Lindt, 2008). Using ultimate fastener capacity data inspected from Dao & van de Lindt (2008), a 10,000 data point array with an approximate Gaussian distribution, a mean value of 689 N and a standard deviation of 80 N was assembled. A histogram of the values can be seen in Figure 18 with the approximate normal distribution. Maximum and minimum values, 917

N and 466 N, respectively, are similar to Dao & van de Lindt's (2008) values and distribution.

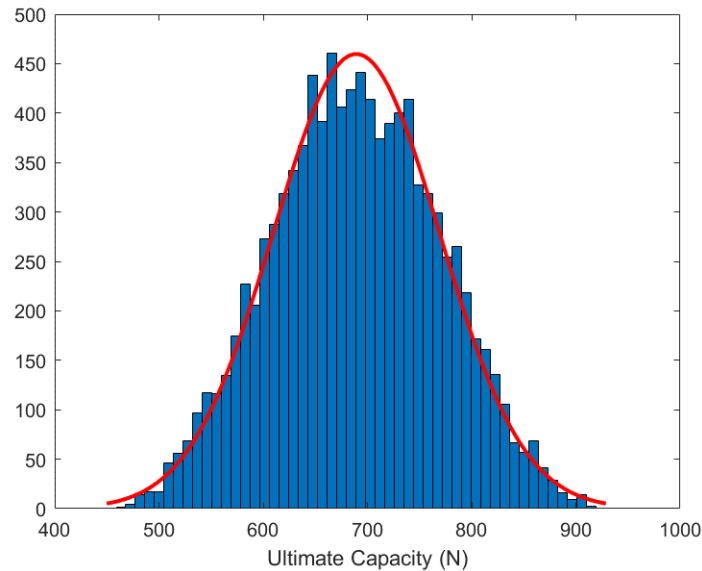


Figure 18: Approximate distribution and histogram of ultimate fastener capacity used in finite element model

During model set up, a uniformly distributed randomly generated index value (0 to 10,000) would be selected and the corresponding value in that array index would be assigned as the ultimate capacity of the link. When comparing ultimate capacities generated using the array, it was found that generated ultimate capacity values had no correlation to others generated for the same panel, row, or among different test runs. As such randomly generated ultimate capacity values were determined to be independent of one another. Yield capacity of the link would then be calculated by subtracting a uniformly distributed random value between 30 and 140 N, the inspected range of values between yield and ultimate capacity values in Dao & van de Lindt (2008), from the randomly generated ultimate capacity. This process was done for all links within the model to replicate the random nature of fastener capacity in a roof sheathing panel. However, when considering randomness in the variation of the displacement associated with the yield and ultimate capacities, numerical instability occurred creating convergence issues within the program. To create more numerical stability all yield

capacities have a displacement of 4 mm and ultimate capacities have a displacement of 34 mm. For further numerical stability a plateau and softening range was defined after link failure. A compression component was also defined to ensure links did not compress under dead or fluctuating loads. A sample definition of a link force-deformation curve can be seen in Figure 19. This was defined for all links as a deformation of $1.0(10^{-4})$ mm for a force of -100 kN (according to local axis orientation).

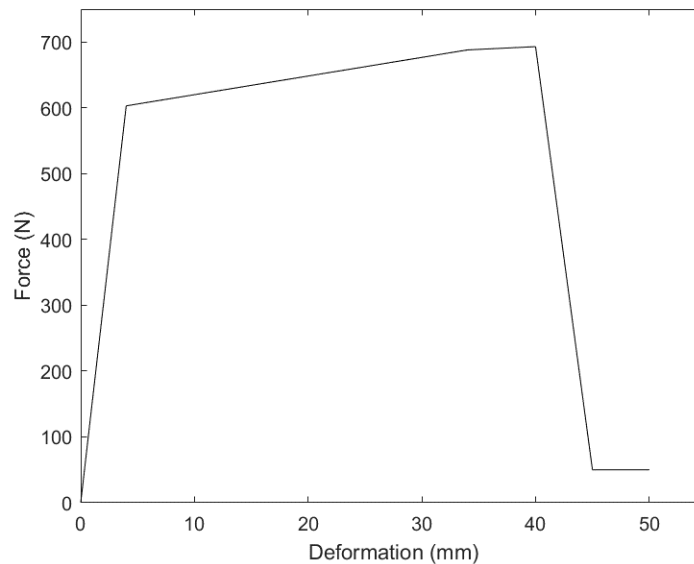


Figure 19: Sample of average fastener link force-displacement curve

To accurately simulate the fasteners connecting the OSB sheathing to the SPF trusses, a double node concept is applied to the finite element model. This double node concept allows the multi-linear plastic link to connect the centroid of the shell elements, representing the OSB sheathing, to the centroid of the frame elements, simulating the SPF trusses. Figure 20 depicts this connection where the blue represents the centroid of the truss, red represents the centreline of the sheathing panel, and the green represents the link. Additional conditions were then set at the nodes to ensure accurate behaviour including rotational restraints at the bottom node to resist lateral movement and rotation of the links.

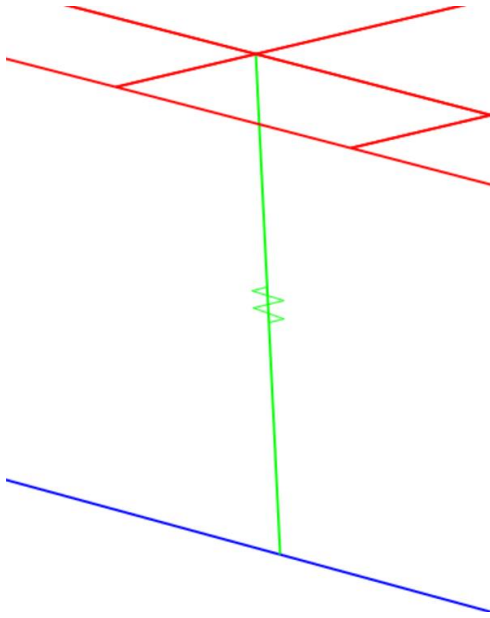


Figure 20: Sample of two node link

Location of the links was predetermined by fastening schedules, those being studied include 6 in by 12 in (150 mm by 300 mm), 6 in by 6 in (150 mm by 150 mm), and 3 in by 3 in (75 mm by 75 mm). Links located at the edge of the panel were drawn 8 mm inside the edge like the location requirements of Henderson, et al. (2013b). Location of the links was defined by a letter-number coordinate system where the letter represented the truss, labeled left to right, A through E, while numbers represented how far up the truss the link was, labeled bottom to top, 1 through 9, the grid system is depicted below in Figure 21. Links for the 6 in by 12 in fastening schedule were located at grid intersections as indicated by the green circles.

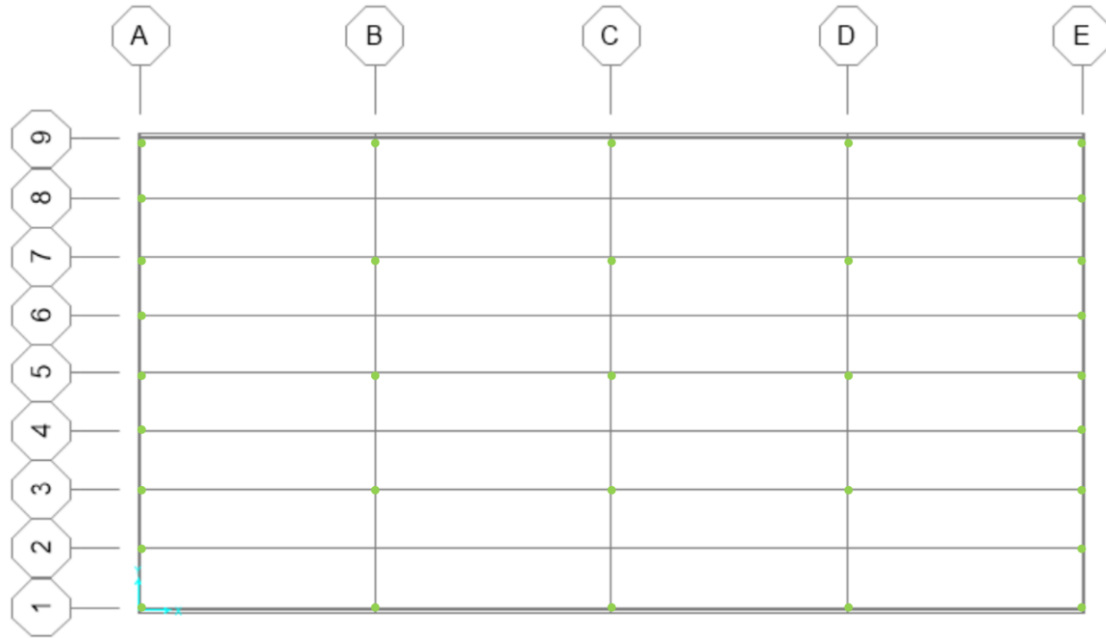


Figure 21: Grid system and link coordinates for finite element model

2.1.4 Time History Loading

To predict the behaviour of a sheathing panel under uplift wind loading, different time histories simulating different types of uplift pressures were considered. Using force control, this can be simulated in SAP2000 by defining a time history function and linking it to an applied load pattern. The time history function acts as an amplification factor for the applied load pattern; for instance, if a unit load (1kPa) is uniformly applied as a shell uniform pressure in the positive z-direction and subject to a time history, the load the panel will experience is the sum of the value of the time history and the unit load. The time history function and applied load pattern are linked through a time history nonlinear analysis load case. Several cases were used in experimentation with a variety of load patterns that are detailed below.

2.1.4.1 Uniform Ramp Loading

The base case for the experimental model is a uniform ramping load. This test method is used in physical experiments to determine sheathing panel capacities and was used for comparison to the fluctuating loads by Henderson et al. (2013b). During the experiments conducted by Henderson et al. (2013b), sheathing panels were uniformly loaded at 0.32

kPa/second. To replicate this, a uniform unit (1kPa) surface pressure was applied in the positive z direction to all shell elements and then linked with a linear time history function increasing at 0.64 per second. Rate of loading did not impact results due to fine data collection resolution, as such it was doubled to reduce computation time. Results from this test can be compared directly to physical experiments as well as fluctuating model loads to determine coherence between loading types.

2.1.4.2 Uniform Fluctuating Load

Similarly, a fluctuating load was applied to the uniform unit surface pressure. The fluctuating time history function was defined using 900 second segment of pressure data, as shown in Figure 22 where negative pressure represents a suction load. The time history consisted of 47,700 points one occurring every 0.0189 seconds. However, this time series created computation issues, so the time history was modified to extend the loading and unloading to a maximum of 0.05 kPa/second and remove regions where the fluctuations in the load did not cause more deformation in the links. An additional ramp was added to the start of the time history to start the simulation from an unloaded state. The modified time history shown in Figure 23 consists of 1000 points 0.01 seconds apart and captures the initial failure pressure. This can be compared to experimentation as well as validate the accuracy of using ramp loading as an effective method for determining initial failure pressure.

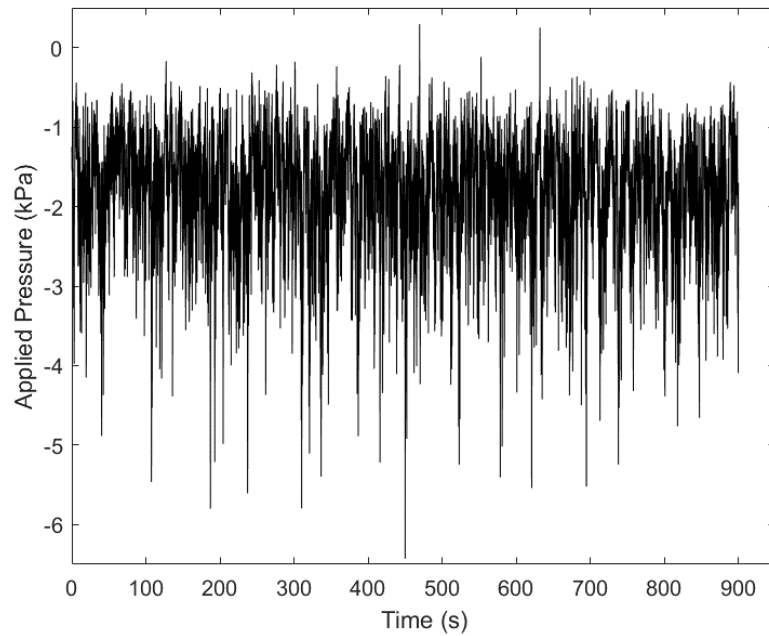


Figure 22: Trace box pressure data for fluctuating wind at 140 mph

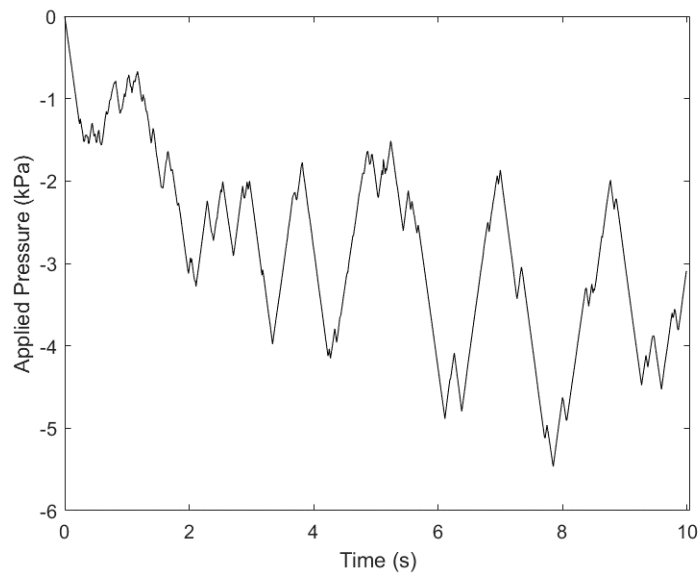


Figure 23: Modified Time History for Finite Element Model Fluctuating Load

2.1.4.3 Point Ramp Load

To determine the lower bound of effective wind area, a point load test was conducted.

The same linearly increasing function of 0.64 per second from the uniform ramp load was

used and applied to a singular unit point load (1kN) acting at the location of the central link C5. This scenario demonstrates that isolated loading of links creates an impact on surrounding links. This leads to load sharing with the smallest possible effective wind area.

2.1.4.4 Spatially-Varying Ramp Load

To replicate realistic wind loading, a spatially-varying load was applied using ASCE 7-16 external pressure coefficients for roof. ASCE 7-16 (2017) Figures 30.3-2A through 30.3-2I use semi-logarithmic graphs to display values of GC_p , external pressure coefficients. To ensure conservative estimations of effective wind area, the worst case was used to define the varying properties. Maximum GC_p values were noted for hip roofs with overhang, roof pitch between 27° and 45° and a height less than 60 ft (18.3 m), of which zone 3 has the largest coefficients, as depicted in Figure 4 and Figure 5 (ASCE 7-16, 2017). Since the sheathing panel model is being assessed as an isolated system, values for GC_p need a greater resolution than 5 sq ft, the smallest area listed for zone 3 in ASCE 7-16 (2017). The minimum effective wind area noted in ASCE 7-16 figures was determined by pressure tap resolution at the time, whereas in reality the trend continues to increase as effective wind area approaches zero. Using the two defined points on the linear portion of the semi-logarithmic chart, $-4.4 GC_p$ at 5 sq ft and -1.8 at 50 sq ft, a function was created to extrapolate the data:

$$GC_p = 1.129 \ln(A_E) - 5.4173 \quad (7)$$

where smaller effective wind area values were used to define a spatially-varying load. Values can be seen in Table 3. These values were then plotted according to Figure 24 and linked with the same linear loading rate of 0.64 per second.

Table 3: Extrapolated ASCE 7-16 GCP values for zone 3 of hip roofs of pitch 27° to 45° with height less than 60 ft (18.3 m)

Effective Wind Area (sq ft)	0.1	0.2	1.0	3.9	8.9	16	32
Effective Wind Area (m ²)	0.006	0.02	0.09	0.37	0.82	1.49	2.98
G _{Cp}	-8.55	-6.98	-5.42	-3.85	-2.94	-2.29	-1.50

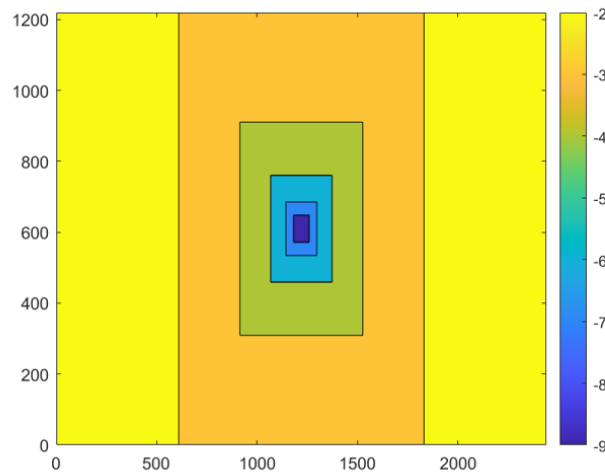


Figure 24: Layout of applied pressure for spatially-varying load case

2.1.5 Finite Element Model Validation

Modelling is a powerful engineering tool when used correctly. To ensure accurate results a validation process against similar physical experiments should be done both qualitatively and quantitatively. The initial validation of the model involves confirming whether modelled sheathing capacities and behaviour of fasteners matches the results in Henderson et al. (2013b).

Quantitative comparison can be done using direct comparisons to sheathing capacities under uniformly applied ramp and fluctuating loading. Henderson et al. (2013b) used pressure loading actuators to determine the failure capacities of roof sheathing under both ramping and fluctuating loads. Failure was defined as the point in which sheathing was disconnected from the truss system; thus, capacity results are the ultimate limit state of

the sheathing panel. For comparison the model's failure is defined as the point of initial failure of a single fastener. This is considered a reasonable estimate due to the rapid succession of failure from one fastener to the entire panel. Henderson et al (2013b) found mean results for OSB sheathing under ramp loading were 4.00 kPa, 4.14 kPa, and 4.66 kPa, with corresponding standard deviations of 0.57 kPa, 0.60 kPa, and 0.65 kPa for coated ring shank, twist shank, and ring shank nails, respectively (Henderson et al., 2013b). Values for these fasteners are of importance for validation as the current model utilizes 8d box nails. Simulated model results under the ramp loading case found the mean initial failure pressure to be 4.63 kPa, falling within the range of nailed fasteners from Henderson, et al. (2013b), but with a standard deviation of 0.14 kPa. Similarly, the ultimate capacity from physical experimentation by Henderson et al. (2013b) under fluctuating loads was 4.06 kPa, 4.25 kPa, and 4.73 kPa, with standard deviations equal to 0.46 kPa, 0.31 kPa, 0.18 kPa, for twist shank, coated ring shank, and ring shank nails, respectively. Failure of the model was determined to have a mean of 4.66 kPa a standard deviation of 0.13 kPa. Thus, mean values of failure capacity for Henderson et al. (2013b) and the current model are similar. However, standard deviations were much smaller in the finite element model. The finite element model accurately represents the capacity of sheathing panels under uplift pressures when compared to physical experimentation. Agreement of mean values of failure capacity from uniform ramp and fluctuating loads in the finite element model also lead to the conclusion that ramp loading is an accurate representation of capacity, similar to the conclusion drawn by Henderson et al. (2013b).

Ensuring accurate replication also involves a qualitative investigation into behaviour exhibited under loading. Specifically, the behaviour of fasteners under fluctuating loading was checked to ensure accurate results from the finite element model. While the finite element model definition of fasteners varies from physical experimentation due to program restraints, similar behaviours during loading and unloading should be exhibited. Beyond the yield capacity under fluctuating loading, the fastener will undergo cyclic behaviour where plastic deformations are maintained during unloading while local deformation follows the linear elastic curve, as seen in Figure 6. This behaviour is also seen in the finite element model during the modified time history runs as shown in Figure 25 below. The similar behaviour of the finite element model's force-displacement figure

to pressure-displacement plots from Henderson et al. (2013b) validate that the behaviour of the fasteners is also accurately representing physical deformation behaviour.

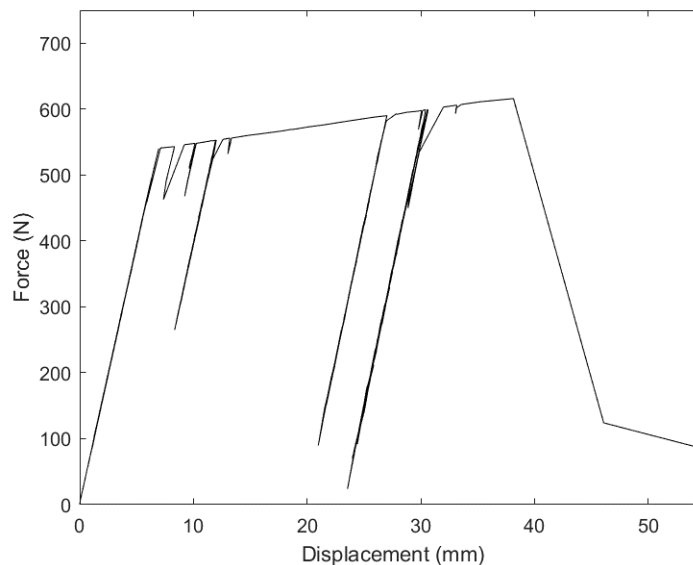


Figure 25: Sample force-deformation behaviour from finite element model

2.1.6 Test Matrix and Monte Carlo Simulation

After model validation, multiple test cases were selected to determine the effective wind area of a sheathing panel. The 6 in by 12 in (150 mm by 300 mm) fastener spacing set up was used as the base case, since it is the minimum allowable fastening schedule in both the AWC WFCM (2015) and NBCC (2015), as well as being the most common in North America. To determine if effective wind area is a function of fastener spacing, other more stringent fastening schedules were also investigated including 6 in by 6 in (150 mm by 150 mm) and 3 in by 3 in (75 mm by 75 mm). Comparing the three cases can also help determine if smaller fastening schedules actively improve panel capacity under uplift loading. To define the boundaries of effective wind area, 3 loading cases are considered: uniform ramp loading, point ramp loading, and spatially-varying ramp loading.

Examining the effect of an individual point load at the central link has on the panel performance allows for a lower bound of effective wind area to be determined. Although the loading is unrealistic, the simplistic loading case shows the minimum load sharing that can occur and the effective area, or area engaged during failure. While uniform ramp

loading provides an upper bound in which effective area should be maximized due to equal loading of all fasteners according to the tributary area method. This test also mimics how ultimate panel capacity is determined through standardized tests and can be directly correlated to their results. Finally, a spatially-varying load, defined using worst-case ASCE 7-16 (2017) GC_P figures was selected as it most accurately reflects real wind loading behaviour on roof sheathing panels. This test is also estimated to be the most accurate in predicting effective wind area. Testing the aforementioned fastening schedules will provide a range of predicted effective wind area and determine its behaviour under common schedules in higher wind risk regions. A matrix of testing cases can be found below in Table 4. Current practice dictates that fasteners and fastening schedules are selected based on the force taken by the geometric tributary area method. This method fails to quantify group action and as a result is over conservative. Using the above tests, the effective wind area will be determined including bounds and a most accurate estimate.

Table 4: Experiment Test Matrix

	6 x 12 (150 x 300)	6 x 6 (150 x 150)	3 x 3 (75 x 75)
Uniform Fluctuating Load	Validate model with real testing		
Uniform Ramp Load	<p>Validate model with real testing</p> <p>Explore load sharing under typical testing</p> <p>Relate nail to panel capacity under load case and maximum effective wind area at standard fastener spacing</p>	<p>Explore load sharing under typical testing with more stringent fastening</p> <p>Relate nail to panel capacity under load case and maximum effective wind area at 6 x 6 spacing</p>	<p>Explore load sharing under typical testing under most stringent fastening</p> <p>Relate nail to panel capacity under load case and maximum effective wind area at 3 x 3 spacing</p>
Point Ramp Load	Define minimum effective wind area at standard fastener spacing	Define minimum effective wind area and explore how it changes with fastener spacing	Define minimum effective wind area and explore how it changes with fastener spacing
Spatially-Varying Ramp Load	Determine a most accurate effective wind area at standard fastener spacing	Determine a most accurate effective wind area and explore how it changes with fastener spacing	Determine a most accurate effective wind area and explore how it changes with fastener spacing

Chapter 3 Results and Analysis

3.1 Initial Failure Force Results

Using the finite element model detailed in the previous chapter the point of failure was determined. For this thesis, failure of the model refers to the failure of the first link. Link failure was determined by meeting the maximum displacement of 34 mm as defined above taken from Dao & van de Lindt (2008). This failure was determined to be a good approximation of ultimate panel failure capacity when comparing to Henderson et al's (2013b) experimental results and the rapid 'unzipping' progressive failure that occurs after the initial link. Once the maximum displacement was achieved the time step was noted and the associated failure force (C_{Fail}) was calculated using various methods for the 3 load cases. Failure force refers to the total force acting on the panel at the point of first link failure. Total panel force for the uniform ramp load was calculated taking the product of the failure time and the ramp time history rate as shown in the equation:

$$F_{uniform} = 0.64TA_{panel} \quad (8)$$

where 0.64 is the ramp time history rate, T is the time of failure, and A_{panel} is the total area of the panel (32 sq ft (2.97 m²)). The point ramp load case the total failure force was the product of the time of first link failure and the time history ramp rate. Calculation of total failure force for the spatially-varying load case required the use of a spatially-varying factor to sum the total panel force. The spatially-varying factor was calculated using:

$$f_{sv} = \Sigma (GC_P)A_A \quad (9)$$

where GC_P is the applied external pressure coefficients and A_A is their associated areas, with the resultant factor being 6.701 kN. This factor was then used to calculate the total failure force of the spatially-varying load case with:

$$F_{sv} = 0.64Tf_{sv} \quad (10)$$

where 0.64 is the time history ramp rate and T is the time of failure. Discussion of the calculated failure forces will be in the following section.

Comparison of results across constant fastener spacing can determine if the initial failure capacity and hence, effective wind area, trends towards the upper or lower bounds of the experimental range. Doing so across the various tested fastener spacing will determine if this trend continues or changes as fasteners are placed closer together. This will also allow the degree of benefit smaller fastener spacing has on effective wind area to be noted. The distributions of initial failure capacity for 6 in by 12 in spacing can be seen in Figure 26, 6 in by 6 in spacing can be found in Figure 27, and 3 in by 3 in spacing can be found in Figure 28. This section will focus on failure capacities of the sheathing panels for the various fastening schedules, calculations for effective wind area can be found in a later section.

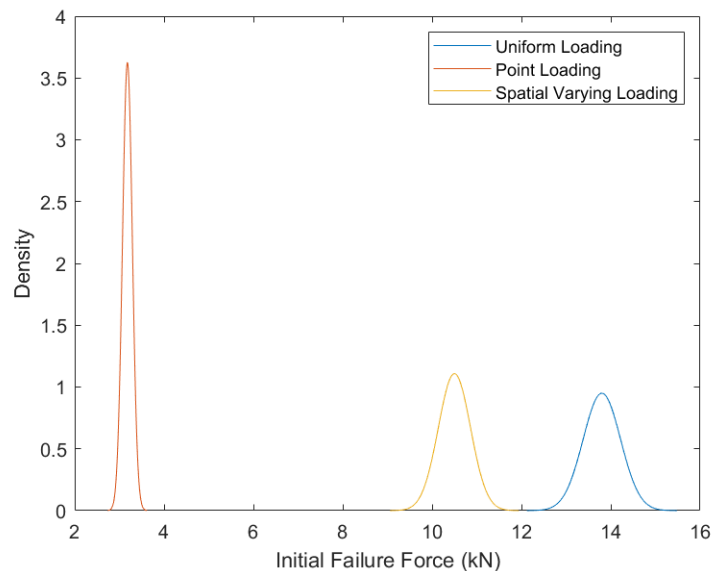
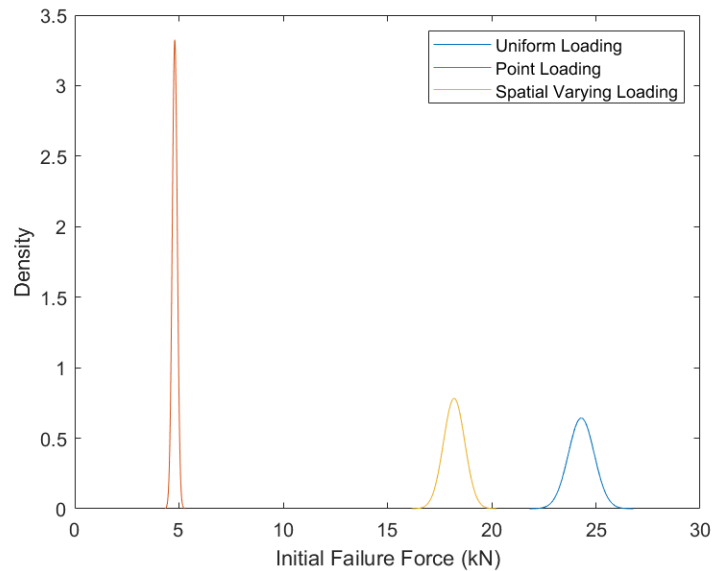


Figure 26: Distributions for three load cases for a 6 in by 12 in fastening schedule

Using code standard spacing of 6 in by 12 in allows the most common and minimum allowable fastening schedule to be examined. Results for the failure force for a 6 in by 12 in fastening schedule are shown in Table 5. For all load cases the standard deviation was respectively small and less than the capacity of the average fastener ultimate capacity. As a result the mean values of the loading cases are a good representation of the failure capacity.

Table 5: Failure force results for 6 in by 12 in fastener spacing

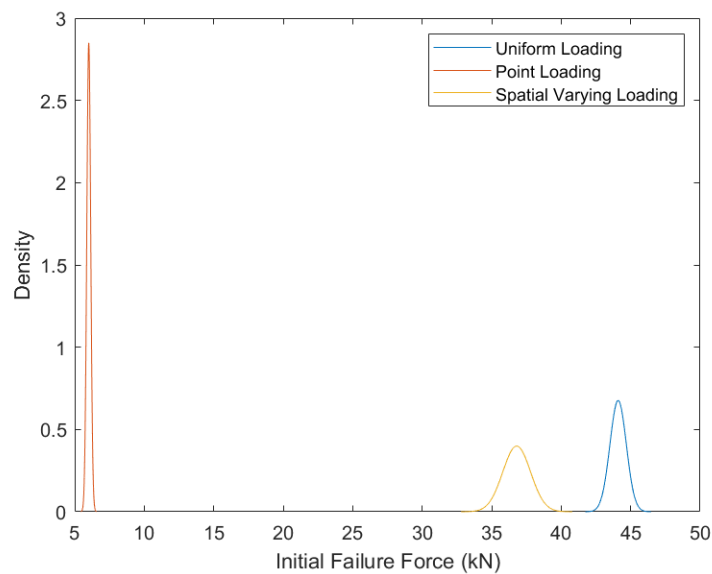
	Uniform	Point	Spatially-Varying
Mean (kN)	13.8	3.18	10.5
Standard Deviation (kN)	0.42	0.11	0.36

**Figure 27: Distributions for three load cases for a fastening schedule of 6 in by 6 in**

More stringent fastening schedules increase the failure capacity of roof sheathing panels, the same was seen using the finite element model. Failure force for the 6 in by 6 in fastening schedule can be seen in Table 6. Standard deviations were larger than that from the 6 in by 12 in fastening schedule but were still less than a single fastener. At a smaller fastening schedule the spatially-varying ramping load case more closely resembled to uniform ramp loading which was similar to the standard 6 in by 12 in spacing results shown above.

Table 6: Failure force results for a 6 in by 6 in fastener spacing

	Uniform	Point	Spatially-Varying
Mean (kN)	24.3	4.80	18.2
Standard Deviation (kN)	0.62	0.12	0.51

**Figure 28: Distributions of three load cases for a fastening schedule of 3 in by 3 in**

For the most stringent fastening schedule the spatially-varying ramping load case results trended towards the uniform ramping load case as shown in Table 7. Standard deviations for the uniform ramp and point ramp loads remained similar to the greater fastener space cases but the spatially-varying case became larger, now greater than the average ultimate capacity of a link. This larger standard deviation now means that this variation needs to be considered in effective wind area calculations.

Table 7: Failure force results for a 3 in by 3 in fastener spacing

	Uniform	Point	Spatially-Varying
Mean (kN)	44.1	6.01	36.7
Standard Deviation (kN)	0.59	0.14	0.86

Overall, when comparing the above results a few trends become apparent. When comparing results of initial failure force results across the various fastening schedules initial failure force increases approximately 150% between the 6 in by 12 in to the 6 in by 6 in and the 6 in by 6 in to the 3 in by 3 in. This increase is approximately proportional with the increasing number of fasteners. Standard deviations across all fastening schedules for the point ramp load case remained small, indicating failure was closely linked to the capacity of the central link and with minimal load sharing occurring. However, the standard deviations for both the uniform and spatially-varying ramp load cases grew as additional fasteners were added indicating that the degree of load sharing varies more. Although the maximum standard deviation is approximately the capacity of a single fastener when fasteners are spaced 3 in apart. This is relatively small as a panel with this fastening schedule has 85 fasteners and a maximum fastener tributary area of 0.5 sq ft.

3.2 Effective Wind Area

Current design practices used in building codes relies on the capacity of individual fasteners to determine overall sheathing panel capacity using the geometric tributary area. This methodology is conservative and fails to consider the interaction between fasteners despite being connected via a sheathing panel. To quantify this load sharing behaviour the area that is engaged at failure should be assessed. Area engaged in failure based on the fasteners involved at that point will define a region that is effective against resisting the uplift loading. This region will be called the effective wind area and can provide a design method that will allow for the benefits of load sharing to be explored. Visual comparison of the area considerations current geometric tributary area method and the proposed effective wind area method can be seen below in Figure 29. In the geometric

tributary area method (Figure 29 A) each fastener is only influenced by their individual tributary area (outlined in red on Figure 29 A), which is based on the spacing between adjacent fasteners. This assumption is conservative and does not consider load sharing. The proposed effective wind area method (Figure 29 B) considers the group action of fasteners within an effective area determined by the number of fasteners fully engaged in failure. For instance, if 9 fasteners were engaged in failure, the resulting effective wind area would be 18 sq ft (example outlined in red on Figure 29 B).

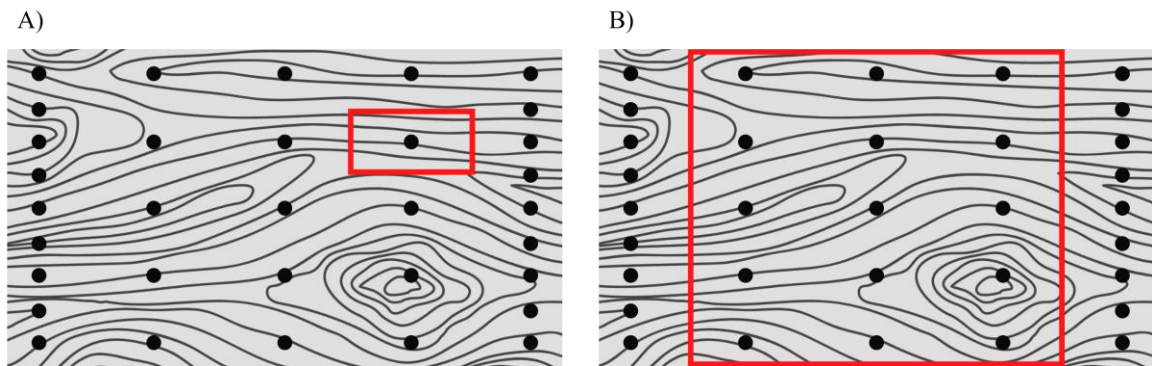


Figure 29: A) Geometric tributary area method for a 6 in by 12 in fastening schedule B) Effective wind area of 9 fasteners engaged in failure for a 6 in by 12 in fastening schedule

Using the initial failure capacity results discussed above the effective wind area can be calculated. The effective wind area is the area that is engaged in the initial failure calculated using the total failure force, and the summation of geometric tributary area of fully engaged fasteners. For example, when a point ramp load is applied to the central link and failure occurs when the point load is equal to the fastener capacity, there is no load sharing. However, if the failure load is double than the individual fastener capacity, two fasteners are involved and there is load sharing.

The process for calculating the effective wind area combines using the sheathing failure capacity, median nail capacity, and geometric tributary area. With the initial failure load (C_{Fail}) determined for all loading cases the number of full fasteners involved in the failure (N) can be calculated. This was done using the fastener capacity distribution (Figure 18) mean (C_{Nails}) of 689 N and the equation below:

$$N = C_{Fail}/C_{Nails} \quad (11)$$

which was then rounded to the nearest whole number. Effective wind area was then calculated using the geometric tributary area of the links engaged in failure using the following equation:

$$A_e = \sum_{i=1}^N A_T \quad (12)$$

where geometric tributary area (A_T), found in Table 8, was summed from largest to smallest as failure initiated at the central link C5. Based on failure progression noted in Henderson et al. (2013b) fasteners on the same truss beside the failure and those on adjacent trusses failed next in succession. This corresponds with links on the central 3 trusses B, C, and D, at the interior positions, which have the largest tributary area. For instance, for the uniform ramp load at 6 in by 12 in fastener spacing a failure load of 13.8 kN was found. Using the mean fastener capacity, it was found that 20 fasteners were fully engaged in the failure. Based on the 6 in by 12 in fastening schedule this means 9 interior fasteners of tributary area 2 sq ft, 6 interior truss-edge fasteners of tributary area 1 sq ft, and 5 exterior truss-interior fasteners of tributary area 0.5 sq ft were engaged. A total of 20 fasteners and an effective wind area of 26.5 sq ft. Values for the rest of the loading cases were calculated and can be found in Table 9 for 6 in by 12 in spacing, Table 10 for 6 in by 6 in spacing, and Table 11 for 3 in by 3 in spacing.

Table 8: Number of Links and Geometric Tributary Area Based on Location

	Internal Truss, Internal Link		Internal Truss, Edge Link		Edge Truss, Internal Link		Edge Truss, Edge Link	
	No. of Links	A _T (sq ft)	No. of Links	A _T (sq ft)	No. of Links	A _T (sq ft)	No. of Links	A _T (sq ft)
6 x 12	9	2	6	1	14	0.5	4	0.25
6 x 6	21	1	6	0.5	14	0.5	4	0.25
3 x 3	45	0.5	6	0.25	30	0.25	4	0.125

Further analysis of results can determine the magnitude of difference between the capacity calculations of current design practice and the proposed effective wind area method. Current code practice uses individual fastener capacities and GC_P values associated with the geometric tributary area to evaluate total panel capacity, as shown in the following equation:

$$q_G = C_{Nail}/(GC_P)_G A_G \quad (13)$$

where q_G represents the allowable dynamic pressure applied when the geometric tributary area is used, $(GC_P)_G$ is the external pressure coefficient minimum of 10 sq ft (or adjusted to 2 sq ft), and A_G is the geometric tributary area. While the effective wind area method can calculate an effective allowable dynamic pressure (q_e) that utilizes group action previously unquantified using:

$$q_e = (C_{Nail}N)/(GC_P)_e A_e \quad (14)$$

where $(GC_P)_e$ is the external pressure coefficient based on the calculated effective wind area, A_e . Two relationships are true between the above calculated pressures:

$$(GC_P)_G > (GC_P)_e \quad (15)$$

and

$$A_G \geq A_e/N \quad (16)$$

which allow the factors causing conservatism in the design loads to be assessed.

Pressures can be converted to wind velocities using air density (ρ) and the following equation:

$$v = \sqrt{(2q/\rho)} \quad (17)$$

where the density of air (ρ) is 1.225 kg/m^3 . These values can then be compared to determine the impact considering load sharing through effective wind area on roof sheathing design. Using the above method of analysis described, values obtained during experimentation can be assessed. These values are also shown below in Table 9, Table 10, and Table 11, respectively for the three fastening schedules.

Assessing the effective wind area for the various load cases at a fastening schedule of 6 in by 12 in produces a range of results. The range is defined by the point ramp load case at the lower limit with an effective wind area of 10 sq ft, while the uniform ramp load case defines the upper limit with an effective wind area of 26.5 sq ft. The spatially-varying ramp load case produced an effective wind area of 24 sq ft, within the bounds but closer to the uniformly loaded case. These values can then be compared to current practice which uses the tributary area of the fasteners to determine GC_P values and associated maximum wind speed. Between the two methods GC_P varies substantially, based on Figure 5 the tributary area method results in a large value of 4.63 at 2 sq ft, as opposed to the effective area method which has values of 1.72, 2.82, and 1.83 for 26.5 sq ft, 10 sq ft, and 24 sq ft, respectively. These values create a dramatic difference in the possible maximum allowable dynamic wind pressure of 0.80 kPa akin to a wind velocity of 80.9 mph or 36.2 m/s for the tributary area method. While using the effective wind area and incorporating load sharing the same panel could increase the maximum allowable dynamic pressure 3.25 kPa corresponding to a wind velocity up to 65 mph at a 6 in by 12 in fastening schedule.

**Table 9: 6 in by 12 in Link Spacing Effective Wind Area Calculation Summary
using Mean Values**

	Uniform	Point	Spatially-Vary.
Capacity (kN)	13.78	3.18	10.52
Nails Involved (N)	20	5	15
Effective Wind Area (sq ft)	26.5	10	24
$(GC_P)_e$	1.72	2.82	1.83
$(GC_P)_G$	4.63	4.63	4.63
Effective Pressure (q_e) (kPa)	3.25	1.21	2.58
Geometric Pressure (q_G) (kPa)	0.80	0.80	0.80
$A_G \geq A_e/N$	$2 \geq 1.28$	$2 \geq 2$	$2 \geq 1.6$
$(GC_P)_G > (GC_P)_e$	$4.63 > 1.72$	$4.63 > 2.82$	$4.63 > 1.83$
“Geometric” Velocity (mph(m/s))	80.9 (36.2)	80.9 (36.2)	80.9 (36.2)
“Effective Velocity” (mph(m/s))	163 (72.9)	99.6 (44.5)	145 (64.9)

When comparing results of the 6 in by 6 in fastening schedule to the 6 in by 12 in schedule, the benefits of more stringent fastening schedules can be discussed. The range of possible effective wind area increases as geometric tributary area of interior fasteners shrink. This is especially noticeable in the point ramp load case where despite more fasteners being engaged in failure, the effective wind area is smaller due to the smaller tributary area. Conversely, the uniform ramp loading case increased the effective wind area and more panel was engaged during the initial failure. However, the size of effective wind area noted by the spatially-varying case remained constant indicating that the critical region envelopes the central 3 trusses, B, C, and D. At this fastening schedule the

use of effective wind area in determining panel capacity could increase maximum wind velocity by 86 mph.

Table 10: 6 in by 6 in Link Spacing Effective Wind Area Calculation Summary using Mean Values

	Uniform	Point	Spatially-Vary.
Capacity (kN)	24.26	4.80	18.24
Nails Involved (N)	35	7	27
Effective Wind Area (sq ft)	28	7	24
$(GC_P)_e$	1.66	3.22	1.83
$(GC_P)_G$	5.42	5.42	5.42
Effective Pressure (q_e) (kPa)	5.62	2.29	4.47
Geometric Pressure (q_G) (kPa)	1.37	1.37	1.37
$A_G \geq A_e/N$	$2 \geq 0.8$	$2 \geq 1$	$2 \geq 0.89$
$(GC_P)_G > (GC_P)_e$	$5.42 > 1.66$	$5.42 > 3.22$	$5.42 > 1.83$
“Geometric” Velocity (mph(m/s))	105 (47.3)	105 (47.3)	105 (47.3)
“Effective” Velocity (mph(m/s))	214 (95.8)	137 (61.2)	191 (85.4)

Similar to the 6 in by 6 in fastening schedule values for the upper and lower bounds of the effective wind area changed. Due to the decreasing tributary area the lower bound continued to shrink to 4.5 sq ft. While the upper bound also became smaller to 27.5 sq ft. This decrease in the upper bound could indicate that under the uniform ramp load case the maximum benefit of effective wind area has been achieved and load sharing is not as effective given the proximity of adjacent fasteners. A slight increase in the effective wind area from 24 sq ft for the 6 in by 6 in and 6 in by 12 in fastening schedules to 24.5 sq ft.

The spatially-varying ramp load case also had a standard deviation which varied the effective wind area by 0.25 sq ft. The variation of the effective wind area was insignificant for further calculations as the GC_P value remained the same. For a 3 in by 3 in fastening schedule using the effective wind area as opposed to the tributary area method could increase maximum wind velocity by 130 mph.

Table 11: 3 in by 3 in Link Spacing Effective Wind Area Calculation Summary using Mean Values

	Uniform	Point	Spatially-Vary.
Capacity (kN)	44.12	6.01	36.67
Nails Involved (N)	64	9	53
Effective Wind Area (sq ft)	27.25	4.5	24.5 ± 0.25
$(GC_P)_e$	1.69	3.72	1.81
$(GC_P)_G$	6.20	6.20	6.20
Effective Pressure (q_e) (kPa)	10.31	3.86	8.93
Geometric Pressure (q_G) (kPa)	2.39	2.39	2.39
Check 1: $A_G \geq A_e/N$	$2 \geq 0.43$	$2 \geq 0.5$	$2 \geq 0.46$
Check 2: $(GC_P)_G > (GC_P)_e$	$6.20 > 1.69$	$6.20 > 3.72$	$6.20 > 1.81$
“Geometric” Velocity (mph(m/s))	140 (62.5)	140 (62.5)	140 (62.5)
“Effective” Velocity (mph(m/s))	290 (130)	178 (79.4)	270 (121)

The direct comparison of the tributary area method and the effective wind area demonstrate the conservative assumptions in current design practice. Effective wind area incorporates load sharing among fasteners which can increase total roof sheathing panel capacity. Current results show that a $7/16$ in OSB sheathing panel has an effective wind

area of 24 sq ft to 24.5 ± 0.25 sq ft. The difference between the two is minimal with GC_p values of 1.83 and 1.81. This demonstrates effective wind area has the same benefit across the 3 fastening schedules investigated, and the minimal benefit gained at the smallest fastening schedule, 3 in by 3 in, also has minimal impact of the GC_p value.

The calculated potential maximum windspeeds also demonstrates the benefit of incorporating load sharing into design of roof sheathing systems. Multiple differences are noted in Table 12 between current code practice and the proposed effective wind area method for the standard 6 in by 12 in fastening schedule include. Current practice assumes independent fasteners as a result maximum wind velocity of 80.9 mph (36.2 m/s) and a large GC_p value of 4.63. While using effective wind area on the same schedule increases the wind velocity for design to 145 mph (64.9 m/s) and the GC_p is lowered to 1.83. By incorporating load sharing among fasteners through effective wind area, designed fastening schedules can become less stringent while maintaining the same capacity calculated using current code assumptions.

Table 12: Comparison of Current Code Practice and Proposed Effective Wind Area Method for a 6 in by 12 in Fastening Schedule

	Current Practice	Proposed Method
Effective Wind Area	2 sq ft	24 sq ft
GC_p	4.63	1.83
Wind Pressure	0.80 kPa	2.58 kPa
Wind Velocity	80.9 mph 36.2 m/s	145 mph 64.9 m/s

3.3 Design Procedure

Using the determined effective wind area for design requires the modification of the usual design procedure. Current practice uses a geometric tributary area method to determine the number of fasteners on the entire panel, assuming each fastener takes a load equivalent to the pressure on the tributary area. The new method uses the effective wind area to determine the capacity and spacing of the fasteners within the effective wind area .

For example, consider a $7/16$ in OSB sheathing panel with 24 inch truss spacing under a wind velocity of 155 mph (69.3 m/s). The dynamic wind pressure is 2.94 kPa. The panel capacity can then be determined using:

$$C_{Fail} = q_e(GC_P)_e A_e \quad (18)$$

where A_e is the calculated effective wind area, 24 sq ft, and $(GC_P)_e$ is the associated external pressure coefficient of 1.83, as found in Figure 5. Thus, the required failure capacity is 12.0 kN acting over the central 24 sq ft. Choosing a fastener with capacity, C_{Nail} , the minimum number of fasteners within the effective wind area can be determined:

$$N_{min} = C_{Fail}/C_{Nails} \quad (19)$$

For C_{Nails} of 689 N the required number of fasteners in the effective wind area is 17. After the minimum number of fasteners has been determined a fastening schedule can be created. For instance, the minimum 17 fasteners above could be increased to 18 with 8 in spacing on the central 3 trusses. This layout is sketched in Figure 30. If a fastener with a higher capacity were chosen, fewer fasteners would be required. It is important to note that the edge fasteners on the panels are often set by shear requirements, rather than uplift. This requirement is often set to be a 6 in spacing. These will still need to be maintained, while ensuring that no 24 sq ft area on the 32 sq ft panel has less than 17 fasteners (in this example).

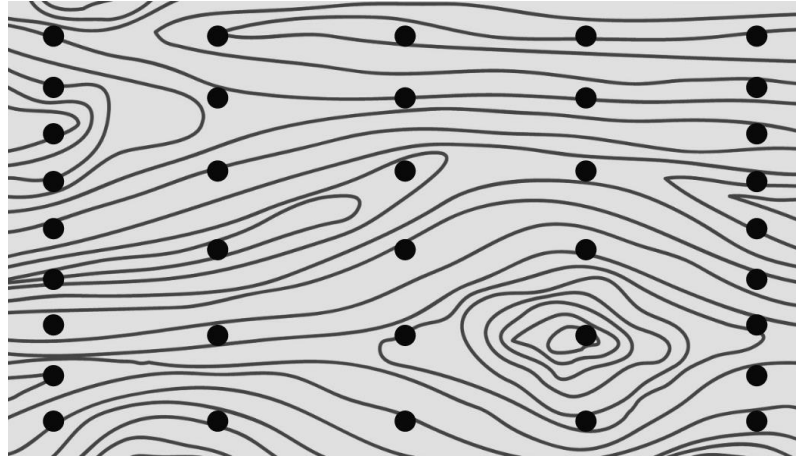


Figure 30: Effective wind area method design procedure example 6 in by 8 in fastening schedule

The modified design procedure reduces the conservatism seen in the current design method by incorporating effective wind area and, thus, load sharing, better reflecting the behaviour of roof sheathing panels in the field. Changes to current design practice will help will allow for more accessible designs in higher risk wind regions.

Chapter 4 Conclusions and Recommendations

Current design practice for cladding systems uses conservative assumptions. Consideration of design loads for extreme wind events, such as tornadoes, merits re-visiting all of the assumptions. Both NBCC (2015) and ASCE 7-16 (2017) use an equivalent static approach for wood-frame structure design under wind loading. Components and cladding, including roof sheathing, are then designed using the equivalent static wind load applied with factors to consider the temporal and spatial variation along the different parts of the structure. These designs typically assume loading that causes the greatest load on the component. To withstand the applied load roof sheathing panels are designed using a geometric tributary area approach. This assumes fasteners are independent and disregards any load sharing behaviour that occurs. In severe windstorm prone regions (or for tornadoes) this can lead to densely packed fastening schedules that are not feasibly possible or split the lumber. This method may underestimate capacity by neglecting the load shared between fasteners. To mitigate this, a more effective design approach that considers load sharing should be considered.

Finite element modelling is a powerful tool used by engineers to assess the behaviour of structures under load. With the high-resolution available, investigation of small components is made easier. Using the finite element software SAP2000 to investigate the initial failure capacity and behaviour of an individual sheathing panel system under uplift loading allows for the determination of an effective wind area. The modelled sheathing panel system included 2 x 4 SPF trusses, $\frac{7}{16}$ in OSB sheathing, and fasteners. Within the model, several considerations are made including the variation of fastener capacity and several different load cases. The load cases explored include a uniform ramp loading case, a point load ramp loading case, and a spatially-varying ramp loading case. The point and uniform ramp loading cases were used to set a bounds of what the effective area could be and it was predicted that the spatially-varying ramp loading would most accurately determine the effective wind area. A uniform fluctuating (time-varying) load case was also used to validate the uniform ramp results accurately reflected this loading. Validation of the model was also done using data from Henderson et al. (2013b) where

mean values obtained from model testing and physical testing were consistent. A Monte Carlo simulation was then used to extract statistical force and deformation results.

The results extracted from the model were then used to confirm equilibrium and calculate the total failure load. Comparison of result distributions across a constant fastening schedule and a constant load case were done to demonstrate the variation of results. For a fastening schedule of 6 in by 12 in (150 mm by 300 mm) mean values were 13.8 kN, 3.18 kN, and 10.5 kN, while standard deviations were 0.42, 0.11, and 0.36 for uniform ramp, point ramp, and spatially-varying ramp loading, respectively. The 6 in by 6 in (150 mm by 150 mm) fastening schedule had means and standard deviations of 24.3 kN, 4.80 kN, and 18.2 kN, and 0.62, 0.12, and 0.51 for uniform ramp, point ramp, and spatial-varying ramp loading, respectively. The 3 in by 3 in (75 mm by 75 mm) spacing under uniform ramp loading had a mean of 44.1 kN and standard deviation of 0.59, while point ramp loading had a mean of 6.01 kN and standard deviation of 0.14, the spatially-varying ramp loading had a mean of 36.7 kN and standard deviation of 0.86. Since the respective standard deviations were small, mean values accurately represented the distribution for calculations of effective wind areas.

Mean values were used to calculate an effective wind area based on the active engaged area at initial failure as determined by fully engaged links. Effective wind area was found to be 24 sq ft (2.23 m²) for a 6 in by 12 in spacing, 24 sq ft (2.23 m²) for the 6 in by 6 in spacing, and 24.5 ± 0.25 sq ft (2.28 m²) for the 3 in by 3 in spacing. This demonstrates that the fastening schedules do not change the effective wind area for the range examined. These values can then be used for design to obtain an appropriate pressure coefficient.

The corresponding pressure and velocity calculated from the effective wind area method when compared with the current code practice method show multiple differences. The most notable was the increase in the allowable design wind speed associated with the effective wind area method which ranged from approximately 60 mph for the 6 in by 12 in fastening schedule to 130 mph for the 3 in by 3 in fastening schedule. The inclusion of load sharing in the effective wind area method allows for less stringent fastening

schedules while maintaining overall panel capacity when compared to current design practices.

The current scope of the project was limited to one type of sheathing and 3 typical fastening schedules. Expanding the research to include other load cases, fastening schedules, and materials could yield different results. For instance, the spatially-varying load case should be changed to have various orientations and sizes. The current experiment was conducted on the thinnest panel allowable $\frac{7}{16}$ in, expanding the project to include thicker sheathing panels is also recommended. Other sheathing panel materials should also be considered as the study was limited to OSB sheathing, this variation of mechanical properties should be investigated to assess differences in load sharing behaviour. Fastening schedules used in this experiment also only included properly inserted nails. Future studies should look into the behaviour of missed or improperly embedded fasteners at various locations to study the impact on load sharing behaviour and panel capacity. Further research should also investigate values for total panel failure capacity. Due to program constraints initial failure of a link was taken as the capacity of the sheathing panel, while this was determined to be accurate it varies slightly with total panel failure and should be investigated. Though these were not covered by the current scope they are important elements to quantify to obtain the full range of effective wind area.

References

- 2015 Special design provisions for wind & seismic. (2015). Leesburg, VA: American Wood Council.
- 2015 Wood frame construction manual for one- and two-family dwellings. (2015). Leesburg, VA: American Wood Council.
- 2018 National design specification for wood construction. (2018). Leesburg, VA: American Wood Council.
- 2018 Supplement National design specification design values for wood construction. (2018). Leesburg, VA: American Wood Council.
- American Society for Testing and Materials (ASTM). (2014). Standard Practice for Establishing Design Capacities for Oriented Strand Board (OSB) Wood-Based Structural-Use Panels (ASTM D 7033). Retrieved from <https://compass.astm.org/>
- ASTM. (2017). Standard Test Method for Determining Bending Yield Moment of Nails (ASTM F 1575). Retrieved from <https://compass.astm.org/>
- ASTM. (2017). Standard Test Methods for Structural Panels in Flexure (ASTM D 3043). Retrieved from <https://compass.astm.org/>
- ASTM. (2019). Standard Test Method for Determining Bending Yield Moment of Staples (ASTM F 3359). Retrieved from <https://compass.astm.org/>
- ASTM. (2020). Standard Test Methods and Definitions for Mechanical Testing of Steel Products (ASTM A 370). Retrieved from <https://compass.astm.org/>
- ASTM. (2020). Standard Test Methods for Mechanical Fasteners in Wood and Wood-Based Materials (ASTM D 1761). Retrieved from <https://compass.astm.org/>
- ASTM. (2020). Standard Test Methods for Nails (ASTM F 680). Retrieved from <https://compass.astm.org/>
- ASTM. (2021). Standard Specification for Driven Fasteners: Nails, Spikes, and Staples (ASTM F 1667). Retrieved from <https://compass.astm.org/>
- Burrows, J. (2014). Canadian wood-frame house construction (3rd ed.). Ottawa: Canada Mortgage and Housing Corporation.
- Cope, A. D., Gurley, K. R., Gioffre, M., & Reinhold, T. A. (2005). Low-rise gable roof wind loads: Characterization and stochastic simulation. *Journal of Wind Engineering and Industrial Aerodynamics*, 93(9), 719-738. doi:10.1016/j.jweia.2005.07.002
- Canadian Standards Association (CSA). (2003). Wire Nails, Spikes and Staples (CSA B111).
- CSA. (2011). Standards on OSB and Waferboard (CSA O437.0).
- CSA. (2014). Engineering design in wood (CSA O86).
- CSA. (2017). Canadian softwood plywood (CSA O151).

- CSA. (2017). Douglas fir plywood (CSA O121).
- CSA. (2019). Poplar plywood (CSA O153).
- CSA. (2021). Construction sheathing (Adopted NIST PS 2-18, with Canadian deviations) (CSA O325).
- Dao, T. N., & Van de Lindt, J. W. (2008). New Nonlinear Roof Sheathing Fastener Model for Use in Finite-Element Wind Load Applications. *Journal of Structural Engineering*, 134(10), 1668-1674. doi:10.1061/(asce)0733-9445(2008)134:10(1668)
- Davenport, A. G. (1967). Gust Loading Factors. *Journal of the Structural Division*, 93(3), 11-34. doi:10.1061/jsdeag.0001692
- Ellingwood, B. R., Rosowsky, D. V., Li, Y., & Kim, J. H. (2004). Fragility Assessment of Light-Frame Wood Construction Subjected to Wind and Earthquake Hazards. *Journal of Structural Engineering*, 130(12), 1921-1930. doi:10.1061/(asce)0733-9445(2004)130:12(1921)
- Gavanski, E., & Kopp, G. A. (2017). Fragility Assessment of Roof-to-Wall Connection Failures for Wood-Frame Houses in High Winds. *ASCE-ASME Journal of Risk and Uncertainty in Engineering Systems, Part A: Civil Engineering*, 3(4), 04017013. doi:10.1061/ajrua6.0000916
- Gavanski, E., Kopp, G. A., & Hong, H. (2014). Reliability analysis of roof sheathing panels on wood-frame houses under wind loads in Canadian cities. *Canadian Journal of Civil Engineering*, 41(8), 717-727. doi:10.1139/cjce-2013-0549
- Gavanski, E., Kordi, B., Kopp, G. A., & Vickery, P. J. (2013). Wind loads on roof sheathing of houses. *Journal of Wind Engineering and Industrial Aerodynamics*, 114, 106-121. doi:10.1016/j.jweia.2012.12.011
- Gill, A., Genikomsou, A. S., & Balomenos, G. P. (2021). Fragility assessment of wood sheathing panels and roof-to-wall connections subjected to wind loading. *Frontiers of Structural and Civil Engineering*, 15(4), 867-876. doi:10.1007/s11709-021-0745-5
- He, W. (2010). Numerical Assessment of Roof Panel Uplift Capacity under Wind Load [Doctoral dissertation]. University of Western Ontario.
- He, J. S., Pan, F. S., & Cai, C. S. (2019). Modeling wind load paths and sharing in a wood-frame building. *Wind and Structures*, 29(3), 117-194. doi:10.12989/was.2019.29.3.177
- He, W., & Hong, H. (2012). Probabilistic characterization of roof panel uplift capacity under wind loading. *Canadian Journal of Civil Engineering*, 39(12), 1285-1296. doi:10.1139/12012-114
- Henderson, D. J., Morrison, M. J., & Kopp, G. A. (2013a). Response of toe-nailed, roof-to-wall connections to extreme wind loads in a full-scale, timber-framed, hip roof. *Engineering Structures*, 56, 1474-1483. doi:10.1016/j.engstruct.2013.07.001

- Henderson, D., Williams, C., Gavanski, E., & Kopp, G. A. (2013b). Failure mechanisms of roof sheathing under fluctuating wind loads. *Journal of Wind Engineering and Industrial Aerodynamics*, 114, 27-37. doi:10.1016/j.jweia.2013.01.002
- Holmes, J. D. (2004). *Wind Loading of Structures*. New York, NY: Spon Press.
- Kopp, G. A., & Gavanski, E. (2012). Effects of Pressure Equalization on the Performance of Residential Wall Systems under Extreme Wind Loads. *Journal of Structural Engineering*, 138(4), 526-538. doi:10.1061/(asce)st.1943-541x.0000476
- Kopp, G. A., Hong, E., Gavanski, E., Stedman, D., & Sills, D. M. (2017). Assessment of wind speeds based on damage observations from the Angus (Ontario) Tornado of 17 June 2014. *Canadian Journal of Civil Engineering*, 44(1), 37-47. doi:10.1139/cjce-2016-0232
- Kopp, G. A., Morrison, M. J., Gavanski, E., Henderson, D. J., & Hong, H. P. (2010). "Three Little Pigs" Project: Hurricane Risk Mitigation by Integrated Wind Tunnel and Full-Scale Laboratory Tests. *Natural Hazards Review*, 11(4), 151-161. doi:10.1061/(asce)nh.1527-6996.0000019
- Kopp, G. A., Morrison, M. J., & Henderson, D. J. (2012). Full-scale testing of low-rise, residential buildings with realistic wind loads. *Journal of Wind Engineering and Industrial Aerodynamics*, 104-106, 25-39. doi:10.1016/j.jweia.2012.01.004
- Lee, K. H., & Rosowsky, D. V. (2005). Fragility assessment for roof sheathing failure in high wind regions. *Engineering Structures*, 27(6), 857-868. doi:10.1016/j.engstruct.2004.12.017
- Martin, K. G., Gupta, R., Prevatt, D. O., Datin, P. L., & Lindt, J. W. (2011). Modeling System Effects and Structural Load Paths in a Wood-Framed Structure. *Journal of Architectural Engineering*, 17(4), 134-143. doi:10.1061/(asce)ae.1943-5568.0000045
- Miller, C. S., Kopp, G. A., Morrison, M. J., Kemp, G., & Drought, N. (2017). A Multichamber, Pressure-Based Test Method to Determine Wind Loads on Air-Permeable, Multilayer Cladding Systems. *Frontiers in Built Environment*, 3. doi:10.3389/fbuil.2017.00007
- Minimum design loads and associated criteria for buildings and other structures (ASCE 7-16). (2017). Reston, VA: American Society of Civil Engineers.
- Mizzell, D. P. (1994). *Wind Resistance of Sheathing for Residential Roofs* [Masters dissertation]. Clemson University.
- Morrison, M. J., Henderson, D. J., & Kopp, G. A. (2012). The response of a wood-frame, gable roof to fluctuating wind loads. *Engineering Structures*, 41, 498-509. doi:10.1016/j.engstruct.2012.04.002
- Morrison, M. J., & Kopp, G. A. (2011). Performance of toe-nail connections under realistic wind loading. *Engineering Structures*, 33(1), 69-76. doi:10.1016/j.engstruct.2010.09.019
- Morrison, M. J., Kopp, G. A., Gavanski, E., Miller, C., & Ashton, A. (2014). Assessment of damage to residential construction from the tornadoes in Vaughan, Ontario, on

- 20 August 2009. *Canadian Journal of Civil Engineering*, 41(6), 550-558.
doi:10.1139/cjce-2013-0570
- Murphy, S., Schiff, s., Rosowsky, D., & Pye, S. (1996). System Effects and Uplift Capacity of Roof Sheathing Fasteners. Structures Congress. ASCE, Worcester, MA, USA
- National building code of Canada. (2015). Ottawa, Ont.: National Research Council Canada, Institute for Research in Construction.
- Parackal, K. I., Ginger, J.D., & Henderson, D. J. (2020). Progressive failures of batten to rafter connections under fluctuating wind loads. *Engineering Structures*, 215, 110684. doi:10.1016/j.engstruct.2020.110684f
- Rosowsky, D. V., & Cheng, N. (1999). Reliability of Light-Frame Roofs in High-Wind Regions. I: Wind Loads. *Journal of Structural Engineering*, 125(7), 725-733. doi:10.1061/(asce)0733-9445(1999)125:7(725)
- Rosowsky, D. V., & Cheng, N. (1999). Reliability of Light-Frame Roofs in High-Wind Regions. II: Reliability Analysis. *Journal of Structural Engineering*, 125(7), 734-739. doi:10.1061/(asce)0733-9445(1999)125:7(734)
- Rosowsky, D. V., & Qingxin, J. (2000). Probability-Based Design of Wood Roof Systems. *Advanced Technology in Structural Engineering*. doi:10.1061/40492(2000)102
- Rosowsky, D. V., & Reinhold, T. A. (1999). Rate-of-Load and Duration-of-Load Effects for Wood Fasteners. *Journal of Structural Engineering*, 125(7), 719-724. doi:10.1061/(asce)0733-9445(1999)125:7(719)
- Rosowsky, D. V., & Schiff, S. D. (1999). Combined Loads on Sheathing to Framing Fasteners in Wood Construction. *Journal of Architectural Engineering*, 5(2), 37-43. doi:10.1061/(asce)1076-0431(1999)5:2(37)
- Sutt, E. G. (2000). The Effect of Combined Shear and Uplift Forces on Roof Sheathing Panels [Doctoral dissertation]. Clemson University.
- Thomas, W. H. (2003). Poisson's ratios of an oriented strand board. *Wood Science and Technology*, 37(3-4), 259-268. doi:10.1007/s00226-003-0171-ykoppf
- van de Lindt, J. W., & Dao, T. N. (2009). Performance-Based Wind Engineering for Wood-Frame Buildings. *Journal of Structural Engineering*, 135(2), 169-177. doi:10.1061/(asce)0733-9445(2009)135:2(169)
- Wood handbook: Wood as an Engineering Material. (2010). Madison, WI: U.S. Dept. of Agriculture, Forest Service, Forest Products Laboratory.

Curriculum Vitae

Name: Nicole Szilagyi

Post-secondary Education and Degrees: The University of Western Ontario
London, Ontario, Canada
2015-2019 B.E.Sc

The University of Western Ontario
London, Ontario, Canada
2019-2022 M.E.Sc

Honours and Awards: Deans Honour List
2015, 2017, 2018

Related Work Experience Graduate Teaching Assistant
The University of Western Ontario
2019-2021